haematologica
Journal of the Ferrata Storti Foundation

CD9 shapes glucocorticoid sensitivity in pediatric B-cell precursor acute lymphoblastic leukemia

by Chi Zhang, Kathy Yuen Yee Chan, Wing Hei Ng, John Tak Kit Cheung, Qiwei Sun, Han Wang, Po Yee Chung, Frankie Wai Tsoi Cheng, Alex Wing Kwan Leung, Xiao-Bing Zhang, Po Yi Lee, Siu Ping Fok, Guanglan Lin, Ellen Ngar Yun Poon, Jian-Hua Feng, Yan-Lai Tang, Xue-Qun Luo, Li-Bin Huang, Wei Kang, Patrick Ming Kuen Tang, Junbin Huang, Chun Chen, Junchao Dong, Ester Mejstrikova, Jiaoyang Cai, Yu Liu, Shuhong Shen, Jun J. Yang, Patrick Man Pan Yuen, Chi Kong Li, and Kam Tong Leung

Received: February 15, 2023.
Accepted: March 22, 2024.

Citation: Chi Zhang, Kathy Yuen Yee Chan, Wing Hei Ng, John Tak Kit Cheung, Qiwei Sun, Han Wang, Po Yee Chung, Frankie Wai Tsoi Cheng, Alex Wing Kwan Leung, Xiao-Bing Zhang, Po Yi Lee, Siu Ping Fok, Guanglan Lin, Ellen Ngar Yun Poon, Jian-Hua Feng, Yan-Lai Tang, Xue-Qun Luo, Li-Bin Huang, Wei Kang, Patrick Ming Kuen Tang, Junbin Huang, Chun Chen, Junchao Dong, Ester Mejstrikova, Jiaoyang Cai, Yu Liu, Shuhong Shen, Jun J. Yang, Patrick Man Pan Yuen, Chi Kong Li, and Kam Tong Leung. CD9 shapes glucocorticoid sensitivity in pediatric B-cell precursor acute lymphoblastic leukemia. Haematologica. 2024 Apr 4. doi: 10.3324/haematol.2023.282952 [Epub ahead of print]

CD9 shapes glucocorticoid sensitivity in pediatric B-cell precursor acute lymphoblastic leukemia

Running Title:
CD9 regulates GC sensitivity

Authors:
Chi Zhang[1], Kathy Yuen Yee Chan[1], Wing Hei Ng[1], John Tak Kit Cheung[1], Qiwei Sun[1], Han Wang[1], Po Yee Chung[1], Frankie Wai Tsoi Cheng[2], Alex Wing Kwan Leung[1], Xiao-Bing Zhang[3], Po Yi Lee[1], Siu Ping Fok[1], Guanglan Lin[1], Ellen Ngar Yun Poon[4], Jian-Hua Feng[5], Yan-Lai Tang[6], Xue-Qun Luo[6], Li-Bin Huang[6], Wei Kang[7], Patrick Ming Kuen Tang[7], Junbin Huang[8], Chun Chen[8], Junchao Dong[9], Ester Mejstrikova[10], Jiaoyang Cai[11], Yu Liu[11], Shuhong Shen[11], Jun J Yang[12], Patrick Man Pan Yuen[1], Chi Kong Li[1,13], Kam Tong Leung[1,13]*****

Affiliations:
[1]Department of Paediatrics, The Chinese University of Hong Kong, Shatin, Hong Kong
[2]Department of Paediatrics and Adolescent Medicine, Hong Kong Children's Hospital, Kowloon Bay, Hong Kong
[3]Haihe Laboratory of Cell Ecosystem, Institute of Hematology & Blood Diseases Hospital, Tianjin, China
[4]School of Biomedical Sciences, The Chinese University of Hong Kong, Shatin, Hong Kong
[5]Department of Hematology, The First Affiliated Hospital of Wenzhou Medical University, Wenzhou, China
[6]Department of Pediatrics, The First Affiliated Hospital, Sun Yat-sen University, Guangzhou, China
[7]Department of Anatomical and Cellular Pathology, The Chinese University of Hong Kong, Shatin, Hong Kong
[8]Division of Hematology/Oncology, Department of Pediatrics, The Seventh Affiliated Hospital, Sun Yat-sen University, Shenzhen, China
[9]Department of Immunology, Zhongshan School of Medicine, Sun Yat-sen University, Guangzhou, China
[10]CLIP-Department of Pediatric Hematology and Oncology, Second Faculty of Medicine, Charles University and University Hospital Motol, Prague, Czech Republic
[11]Department of Hematology/Oncology, Shanghai Children's Medical Center, School of Medicine, Shanghai Jiao Tong University, Shanghai, China
[12]Department of Pharmaceutical Sciences, St. Jude Children's Research Hospital, Memphis, TN, USA
[13]Hong Kong Hub of Paediatric Excellence, The Chinese University of Hong Kong, Shatin, Hong Kong

***Correspondence:**
Kam Tong Leung, PhD
Email: ktleung@cuhk.edu.hk
Address: Research Office, 8/F, Tower A, Hong Kong Children's Hospital, 1 Shing Cheong Road, Kowloon Bay, Kowloon, Hong Kong
Tel: (852) 3513 3176
Fax: (852) 2636 0020

Subject Category: Acute Lymphoblastic Leukemia

Authorship Contributions:

C.Z., K.Y.Y.C., W.H.N., J.T.K.C., Q.S., H.W., P.Y.C., P.Y.L., S.P.F., and G.L. performed the experiments and analyzed the data. F.W.T.C., and A.W.K.L. provided clinical samples and obtained patient consent. X.B.Z., E.N.Y.P., J.H.F., Y.L.T., X.Q.L., L.B.H., W.K., P.M.K.T., J.H., C.C., J.D., E.M., J.C., Y.L., S.S., and J.J.Y. provided advice on study design, contributed to essential laboratory reagents, solicited clinical data, and edited the manuscript. P.M.P.Y., C.K.L., and K.T.L. conceived the study, interpreted the data, wrote the manuscript, and contributed to research funding. All authors have reviewed and approved the final paper.

Funding:

This study was supported by the Bone Marrow Transplant Fund, Hong Kong (project no: 7105113); Children's Cancer Foundation, Hong Kong (project no: 7104593); HOPE Research Seed Fund, The Chinese University of Hong Kong, Hong Kong (project no: HOPE-007); Sanming Project of Medicine, Shenzhen, China (project no: SZSM202011004); IdeaBooster Fund, The Chinese University of Hong Kong, Hong Kong (project no: IDBF23MED11); Ministry of Health, Czech Republic (AZV no: NU23-05-00353); and Direct Grant for Research, The Chinese University of Hong Kong, Hong Kong (project no: 4054491). The funding bodies were not involved in the study design, the collection, analysis, and interpretation of data, or the decision to submit the manuscript for publication.

Conflict of Interest Disclosure:

The authors declare that they have no conflicts of interest.

Data Sharing Statement:

Sequencing data of BCP-ALL cell lines were deposited in Gene Expression Omnibus (GEO; accession number: GSE220979). Sequencing data of patient samples are available from the corresponding author on reasonable request. The data are not publicly available due to privacy or ethical restrictions.

Abstract

Resistance to glucocorticoids (GCs), the common agents for remission induction in pediatric B-cell precursor acute lymphoblastic leukemia (BCP-ALL), poses a significant therapeutic hurdle. Therefore, dissecting the mechanisms shaping GC resistance could lead to new treatment modalities. Here, we showed that $CD9^-$ BCP-ALL cells were preferentially resistant to prednisone and dexamethasone over other standard cytotoxic agents. Concordantly, we identified significantly more poor responders to the prednisone prephase among BCP-ALL patients with a $CD9^-$ phenotype, especially for those with adverse presenting features including older age, higher white cell count and *BCR-ABL1*. Furthermore, gain- and loss-of-function experiments dictated a definitive functional linkage between CD9 expression and GC susceptibility, as demonstrated by the reversal and acquisition of relative GC resistance in $CD9^{low}$ and $CD9^{high}$ BCP-ALL cells, respectively. Despite physical binding to the GC receptor NR3C1, CD9 did not alter its expression, phosphorylation or nuclear translocation but potentiated the induction of GC-responsive genes in GC-resistant cells. Importantly, the MEK inhibitor trametinib exhibited higher synergy with GCs against $CD9^-$ than $CD9^+$ lymphoblasts to reverse drug resistance *in vitro* and *in vivo*. Collectively, our results elucidate a previously unrecognized regulatory function of CD9 in GC sensitivity, and inform new strategies for management of children with resistant BCP-ALL.

Introduction

Acute lymphoblastic leukemia (ALL) is the most common childhood hematologic malignancy, accounting for ~25% of pediatric cancers.[1] The classical treatment protocol comprises sequential phases of remission induction, consolidation, delayed intensification and maintenance, which relies on the risk-directed usage of multiagent therapy including the backbone drugs prednisolone (Pred), dexamethasone (Dex), vincristine (VCR), L-asparaginase (L-ASP), cytarabine (Ara-C), daunorubicin (DNR), methotrexate (MTX) and 6-mercaptopurine (6-MP).[2] Optimal application of these agents, together with refined risk group stratification and appropriate supportive care, has yielded a significant improvement in the overall survival of newly diagnosed pediatric ALL to over 85% in most developed countries.[3,4] However, disease relapse still occurs in 10-20% of patients, with <50% of whom can be cured with salvage regimens, indicating the emergence of drug resistance and requirement for treatment interventions.[5,6]

Glucocorticoids (GCs), including Pred and Dex, are the core therapeutic agents for remission induction in pediatric ALL. In some treatment protocols, patients with a poor response to the Pred prephase were stratified into the high-risk arm to receive intensified multiagent chemotherapy.[7–10] Resistance to GCs is found in 15-30% of newly diagnosed pediatric ALL cases and 70% of relapsed patients.[11] Moreover, specific high-risk subtypes of ALL, including those with *KMT2A* rearrangements or *BCR-ABL1* translocation, tend to have poorer responses to GCs.[12,13] GCs induce apoptosis in malignant lymphoblasts by binding to the glucocorticoid receptor NR3C1. This ligand-activated transcription factor subsequently undergoes phosphorylation, translocates into the nucleus and activates the transcription of GC-responsive genes.[14] Diverse mechanisms have been reported to attribute resistance of ALL to GCs, including but not limited to mutations of the GC receptor NR3C1[15] and coactivator CREBBP,[16] alteration of molecular signaling pathways, such as MAPK,[17] NOTCH1,[18] AKT[19] or AURKB,[20] and deregulation of the BCL-2 family protein BIM.[21] Indeed, the reversal of GC resistance has been considered a potential intervening strategy for further improvement of patient outcomes and is especially important for relapsed ALL.[22] Preclinical investigations have revealed early successes, as demonstrated by the restoration of GC sensitivity in T-cell ALL by the AKT inhibitor MK2206[23] and in B-cell precursor (BCP)-ALL by the MEK1/2 inhibitor trametinib.[17] While some of these agents are scheduled to be evaluated in upfront clinical trials, it is important to further investigate new mechanisms underlying GC resistance, and leverage the knowledge

to develop intervening strategies for high-risk subjects.

CD9, a prototypic member of the tetraspanin family proteins, is involved in many physiologic processes, such as cell migration and adhesion, by forming complexes with other transmembrane or cytosolic proteins into a membrane structure known as the tetraspanin-enriched microdomain (TEM), where the functions of partner proteins are modulated.[24] Substantial evidence also reveals the importance of CD9 in solid and hematologic malignancies, although its nature is context-dependent and cannot be strictly classified as an oncogene or tumor suppressor.[25] Our group previously identified CD9 as a critical effector of hematopoietic stem cell homing[26] and recently also unleashed its prognostic significance in pediatric BCP-ALL.[27,28] To elucidate whether its impact on clinical outcome is related to drug response, we, in this study, further profiled the sensitivity pattern of $CD9^+$ and $CD9^-$ BCP-ALL to frontline therapeutic agents, and discovered its previously unknown linkage with GC susceptibility.

Methods

Full experimental procedures are described in Supplemental methods.

Cells, patient cohort and CD9 characterization

BCP-ALL cell lines were maintained in serum-supplemented RPMI-1640 medium. $CD9^{low}$ cells were transduced with control GFP-only or CD9-GFP lentiviral particles to achieve gene overexpression, whereas $CD9^{high}$ cells were transduced with control sgRNA-Cas9-GFP or CD9 sgRNA-Cas9-GFP to achieve gene knockout.[29] Primary lymphoblasts were recovered from diagnostic samples of pediatric BCP-ALL cases consecutively recruited into three successive clinical studies,[7–9] where patients were unanimously treated with a Berlin-Frankfurt-Münster (BFM)-based protocol with a Pred prephase. All human specimens were obtained with informed written consent and in accordance with procedures approved by the Joint CUHK-NTEC Clinical Research Ethics Committee. Lymphoblasts were characterized for CD9 expression by flow cytometry, with gating strategy shown in Supplemental Figure 1A.

Drug sensitivity assay

BCP-ALL cell lines were treated with DMSO or 0.1 nM-100 μM of Pred, Dex, Ara-C, DNR, VCR, or MTX

for 72 hours. Cell proliferation was measured by MTS assay. A mesenchymal stem cell (MSC)-based drug testing system was adopted to determine the sensitivity of primary lymphoblasts to GCs.[30] Representative flow cytometry plots showing the sequential gating for defining apoptotic lymphoblasts are shown in Supplemental Figure 1B. The half-maximal inhibitory concentrations (IC50s) were calculated from the dose-response curves by nonlinear regression.[31] In some experiments, BCP-ALL cells were concomitantly treated with the indicated doses of trametinib or ruxolitinib to determine their synergy with GCs using the Bliss independence model.[32]

Western blotting and co-immunoprecipitation

Whole cell lysates or subcellular components were recovered from BCP-ALL cells with or without GC treatment. Proteins were separated and detected for CD9, NR3C1, p-NR3C1, MEK1/2, p-MEK1/2, ERK1/2 or p-ERK1/2 by standard SDS-PAGE and immunoblotting procedures. To dictate protein-protein interactions, lysates were immunoprecipitated with CD9 antibody and probed for NR3C1 or TEM components.[24]

RNA-seq, ChIP-seq and quantitative RT-PCR

Total RNA was extracted from patient samples or BCP-ALL cell lines with or without Dex treatment. cDNA libraries were generated and sequenced to curate GC-responsive genes, *NR3C1* isoform expression and *NR3C1* hotspot mutations.[33,34] Chromatin of Dex-treated BCP-ALL cells was precipitated with NR3C1 antibody. Eluted DNA fragments were sequenced to locate and quantify NR3C1 binding.[35] Quantitative RT-PCR was performed with TaqMan-based assays to validate selected GC-responsive genes (Supplemental Table 1).

Xenograft experiments

Animal experiments were conducted in accordance with procedures approved by the Institutional Animal Experimentation Ethics Committee. NSG mice were infused with luciferase-expressing $CD9^{low}$ SEM or $CD9^{high}$ BV-173 cells. On day 3 post-transplantation, animals were randomized to receive a 2-week treatment of vehicle control, Dex (5 mg/kg), trametinib (5 mg/kg) or their combination.[36] At humane

endpoints, systemic and bone marrow leukemic load were measured by bioluminescence imaging and flow cytometry, respectively.

Statistical analyses

The statistical methods applied for individual experiments are indicated in the table footnotes or figure legends. Analyses were performed with GraphPad Prism v8.3.0 or SPSS v26.0. *P* values of <0.05 were considered statistically significant.

Results

BCP-ALL cells with low CD9 expression are resistant to glucocorticoids

To investigate the association of CD9 expression with drug response, we first performed *in vitro* sensitivity profiling of $CD9^{high}$ (697, BV-173, RS4;11 and SUP-B15; cell surface CD9 expression higher than mean) and $CD9^{low}$ BCP-ALL cell lines (KOPN-8 and SEM; cell surface CD9 expression lower than mean) to standard therapeutic agents used in remission induction or consolidation therapy for pediatric BCP-ALL (Figure 1A). Hierarchical clustering analyses revealed distinct drug sensitivity patterns and a clear association with CD9. In cluster A, the BCP-ALL cells, in general, were sensitive to Ara-C, DNR, VCR or MTX, without significant differences in the extent of drug responses between $CD9^{high}$ and $CD9^{low}$ lines. In cluster B, which exclusively contained the two tested GCs, $CD9^{high}$ but not $CD9^{low}$ lines were sensitive to Pred (mean IC50s: 140 *vs.* 19,357 nM, *P*=0.015) or Dex (mean IC50s: 9.0 *vs.* 693 nM; *P*=0.002). We then validated the impact of CD9 on GC responses using primary cells isolated from 18 diagnostic BCP-ALL samples encompassing the major cytogenetic subtypes, with patient characteristics shown in Supplemental Table 2. Concordantly, under a MSC coculture system, lymphoblasts from $CD9^{+}$ cases exhibited markedly higher sensitivity to Pred (median IC50s: 269 *vs.* 8,186 nM; *P*=0.03) or Dex (median IC50s: 31.5 *vs.* 2,761 nM; *P*=0.03) when compared to $CD9^{-}$ cases (Figures 1B and 1C).

CD9 negativity is associated with poor prednisone responses in BCP-ALL patients

We then capitalized on our three clinical studies,[7–9] which commonly adopted a treatment prephase of 7-day Pred before the initiation of multiagent chemotherapy, to retrospectively explore the association of CD9

with early GC responses in pediatric BCP-ALL. A total of 182 children (median age: 4.4 years) were recruited, stratified into $CD9^+$ and $CD9^-$ subgroups (positivity defined by the presence of ≥20% $CD9^+$ blasts; this cutoff consistently showed the strongest prognostic significance in our single- and multi-center studies),[27,28] and compared for Pred responses (poor response defined by the presence of $\geq 1\times10^9$/L circulating leukemic blasts on day 8).[8] In this cohort, 16 patients (8.8%) were poor prednisone responders (Table 1). Consistent with the *ex vivo* drug testing results, more $CD9^-$ patients exhibited poor responses to Pred than $CD9^+$ patients (19.4% *vs*. 6.2%, *P*=0.02). Subgroup analyses further revealed that poor Pred responders with a $CD9^-$ phenotype were significantly enriched in patients with older age (60% *vs.* 3.7%, *P*=0.008), male gender (21.7% *vs.* 6.7%, *P*=0.045), higher white cell count (66.7% *vs*. 15.4%, *P*=0.004) and in those with *BCR-ABL1* translocation (100% *vs.* 12.5%, *P*=0.024) or not otherwise specified BCP-ALL (30.8% *vs*. 5.8%, *P*=0.019). Notwithstanding, there was no significant enrichment of $CD9^-$ patients in these high-risk subgroups (Supplemental Table 3). Univariate analyses revealed that $CD9^-$ phenotype, high white cell count and the presence of *BCR-ABL1* were significantly associated with poor Pred responses. Multivariate analyses further confirmed CD9 negativity as an independent predictive factor for this adverse feature (OR=5.1, *P*=0.009; Supplemental Table 4).

CD9 is definitively linked to glucocorticoid susceptibility

To validate the association of CD9 with GC sensitivity at the functional level, we first employed a gain-of-function approach by transducing $CD9^{low}$ SEM cells with GFP or CD9-GFP lentiviral vectors, resulting in control GFP^+CD9^{low} and experimental GFP^+CD9^{high} stable cell lines (Figure 2A). We then tested their sensitivity to standard therapeutic agents. Convincingly, $CD9^{high}$ SEM cells exhibited 8.9- and 2.8-fold increases in sensitivity to Pred (IC50s: 6,231 nM *vs*. 55,346 nM; *P*=0.017) or Dex (IC50s: 351 nM *vs.* 991 nM; *P*=0.005), respectively when compared with control $CD9^{low}$ cells (Figure 2B). Such differential drug sensitivity was not observed for other cytotoxic agents, except for a modest increase in the sensitivity of $CD9^{high}$ SEM cells to Ara-C (Figure 2C). Similar findings were observed in another $CD9^{low}$ cell line KOPN-8, where experimental GFP^+CD9^{high} cells exhibited 23.5- and 203-fold increases in sensitivity to Pred (IC50s: 2,260 nM *vs*. 53,195 nM; *P*=0.003) or Dex (IC50s: 253 nM *vs*. 51,552 nM; *P*=0.024), respectively (Figure 2D). The overexpression system did not appear supraphysiologic, as reflected by the similar mRNA

and total protein levels of CD9 in CD9-overexpressing cells and cells with inherently high CD9 expression. Yet, the sensitivity of CD9-overexpressing cells to GCs was still lower than $CD9^{high}$ BCP-ALL lines (Supplemental Figures 2A and 2B). We further adopted a loss-of-function approach by transducing $CD9^{high}$ 697 cells with GFP-tagged CRISPR/Cas9 lentiviral vectors bearing non-targeting or CD9-targeting sgRNAs, and generated $GFP^{+}CD9^{high}$ and $GFP^{+}CD9^{low}$ stable cells (Figure 2E). Consistent with our observation that low CD9 expression is linked to GC resistance, CD9 knockout significantly decreased the sensitivity of 697 cells to Pred (IC50s: 348 nM *vs.* 261 nM; P=0.002) or Dex (IC50s: 16.9 nM *vs*. 14.4 nM; P=0.003) compared with control $CD9^{high}$ cells (Figure 2F).

CD9 binds to the glucocorticoid receptor but does not affect its expression, phosphorylation or translocation

To assess whether CD9 alters GC sensitivity *via* the GC receptor, we first measured the basal expression of NR3C1 in BCP-ALL cell lines. NR3C1 protein was ubiquitously expressed in $CD9^{low}$ and $CD9^{high}$ lines despite their differential responses to GCs (Supplemental Figure 3A). There was also no significant difference in the protein expression of NR3C1 between $CD9^{+}$ and $CD9^{-}$ patient samples (Figure 3A). Concordantly, *NR3C1* mRNA expression neither differed between $CD9^{+}$ and $CD9^{-}$ cases nor correlated with *CD9* mRNA levels (Figure 3B). There were also no significant differences in the expression of major *NR3C1* isoforms (GRα, GRβ and GRγ)[37] when stratified by CD9 status. Furthermore, hotspot *NR3C1* mutations associated with GC resistance (p.Y478C and p.R477H)[38] could not be detected in any BCP-ALL cell lines or samples employed in this study (Supplemental Table 5). Parental (Supplemental Figure 3B) or transduced BCP-ALL cells (Supplemental Figure 3C) also had no differences in NR3C1 protein expression upon GC treatment. Besides, GC-induced phosphorylation of NR3C1 at Ser211 and Ser 226[23] was competent in both $CD9^{low}$ and $CD9^{high}$ SEM cells (Figure 3C). Given that GCs induce receptor cytoplasmic-nuclear shuttling,[14] we next evaluated the subcellular level of NR3C1 in transduced BCP-ALL cells. Cytoplasmic to nuclear translocation of NR3C1 was robust upon GC stimulation in both control and CD9-overexpressing SEM cells (Figure 3D) and similarly in the KOPN-8 and 697 systems (Supplemental Figure 3D). CD9 typically exerts its function by binding with other partner proteins,[24] we therefore performed coimmunoprecipitation assay and unexpectedly revealed the physical interaction of CD9 with NR3C1 in

CD9^{high} SEM cells (Figure 3E). This interaction diminished upon GC stimulation, possibly due to the partial detachment and translocation of NR3C1 into the nucleus. The CD9-NR3C1 complex was also found in BCP-ALL lines with inherently high CD9 expression, and precipitated together with well-known CD9 interactors EWI-2 and CD81 within the TEM (Supplemental Figure 4).

CD9 enhances transcription of glucocorticoid-responsive genes

To identify the downstream gene signatures underpinning GC sensitivity, we performed RNA sequencing (RNA-seq) on CD9^{high} and CD9^{low} SEM cells upon GC exposure. After an 8-hour Dex treatment, more differentially expressed genes (DEGs) were found in CD9^{high} than CD9^{low} cells (110 *vs.* 82; Figure 4A). Venn analysis showed that 75 DEGs were commonly regulated by Dex in both CD9^{high} and CD9^{low} cells, whereas 35 DEGs were exclusively altered in CD9^{high} cells (Figure 4B). The complete list of DEGs is shown in Supplemental Table 6, where 28 of them are known GC-responsive genes. We next validated three DEGs, including *ZBTB16* (PLZF), *TSC22D3* (GILZ) and *BCL2L11* (BIM) that are well known GC-responsive genes participating in GC-induced apoptosis or cell cycle progression.[21,39,40] By quantitative PCR, we found that the magnitude of their induction was significantly higher in CD9^{high} cells (P<0.05; Figure 4C). Given that CD9 illuminates a more robust GC-induced gene transcription program despite intact NR3C1 nuclear translocation, we further performed chromatin immunoprecipitation sequencing (ChIP-seq) to assess NR3C1 binding to GC-responsive genes. In both CD9^{high} and CD9^{low} SEM cells, we detected distinct peaks in the glucocorticoid response elements (GRE) of *TSC22D3* and *ZBTB16* upon Dex treatment (Figure 4D), indicating that DNA binding of translocated NR3C1 was competent.

MEK inhibition preferentially increases the susceptibility of CD9^{low} BCP-ALL cells to glucocorticoids

Given that constitutive activation of the MAPK pathway is associated with GC resistance,[17] we assessed the synergism of GCs with the MEK inhibitor trametinib in CD9^{+} and CD9^{-} BCP-ALL cells. Trametinib exhibited a strong synergy with Pred or Dex in CD9^{low} SEM and KOPN-8 cells (excess over Bliss score >0) but antagonism in CD9^{high} RS4;11 and BV-173 cells (excess over Bliss score <0) (Supplemental Figure 5A). Furthermore, in SEM and KOPN-8 cells, CD9 overexpression consistently reduced the synergy between GCs and trametinib (Supplemental Figure 5B). These phenomena were successfully recapitulated with

animal modeling. In $CD9^{low}$ SEM but not $CD9^{high}$ BV-173 xenografts, combined treatment with Dex and trametinib effectively reduced systemic and medullary leukemic load when compared to single-agent treatments ($P<0.05$; Figure 5A). In patient samples, despite their differences in GC sensitivity, we neither observed significant differences in the activation status of the MAPK pathway components between $CD9^+$ and $CD9^-$ cases (Supplemental Figure 6A) nor their correlation with trametinib sensitivity (Supplemental Figure 6B). Consistent with the observations in BCP-ALL cell lines, trametinib only exhibited synergy with Dex in $CD9^-$ but additivity or antagonism in $CD9^+$ cases (Figure 5B), suggesting trametinib may preferentially benefit $CD9^-$ patients. Given that STAT5 and ERK are segregated in BCP-ALL,[41] $CD9^+$ lymphoblasts may escape from the trametinib/GC combination by compensatory activation of the STAT pathway. Coincidentally, the gain of CD9 induced an exclusive upregulation of *STAT5A* in Dex-treated SEM cells ($P=0.023$; Figure 5C). *Ex vivo* drug testing showed that the JAK inhibitor ruxolitinib tended to provide an additional degree of leukemia suppression in the background of trametinib/Dex combination in $CD9^+$ cases (Figure 5D).

Discussion

In this study, we have established a previously unknown linkage between CD9 and GC sensitivity in pediatric BCP-ALL and informed pharmacologic approaches guided by CD9 status to reverse GC resistance. Our data not only uncover a new biological function of CD9 but also implicate improved strategies for the management of this childhood malignancy.

By drug sensitivity profiling of BCP-ALL cells, we identified an apparent association of CD9 negativity with GC resistance. This phenomenon is specific to GCs but not to other cytotoxic agents. Notably, the respective reversal and acquisition of relative GC resistance upon CD9 overexpression and knockout further provided definitive proof for its genuine control of GC susceptibility. Similar to its well-documented oncogenic and tumor suppressive functions,[25] CD9 can exert context-dependent regulation of drug sensitivity in different cancer types. In multiple myeloma, downregulation of CD9 by DNA methylation was functionally linked to bortezomib resistance.[42] In contrast, increased expression of CD9 in breast cancer was responsible for resistance to doxorubicin and 5-fluorouracil by modulating the crosstalk between tumor cells and MSCs.[43] Likewise, preferential expression of CD9 in metastatic small cell lung cancer mediated

resistance to etoposide and cisplatin *via* activation of β1 integrin.[44] These findings, together with ours, illustrate the complex nature of CD9 in regulating drug responses, where both cell adhesion-dependent and -independent mechanisms may concurrently exist. Indeed, the linkage of CD9 to GC resistance was consistently observed in both leukemia monocultures and MSC cocultures, suggesting that the effects of CD9 on GC responsiveness in BCP-ALL are possibly regulated by cell-intrinsic mechanisms.

In a cohort of pediatric BCP-ALL patients, we found that CD9 negativity independently predicted poor Pred responses. Interestingly, Pred non-responders were mostly enriched in $CD9^-$ patients with older age, higher white cell count, male gender and *BCR-ABL1*. Although these are also recognized risk factors for poor Pred response that might potentially confound the interpretation, CD9 negativity still stood out as an independent predictive factor in multivariate analyses. Given that some consortia have adopted multiple drug induction without Pred prephase in newer treatment protocols,[4,45] CD9 expression status at diagnosis could therefore serve as a surrogate marker for initial risk stratification. Our previous study contradictorily identified that CD9 positivity was associated with inferior survival in pediatric BCP-ALL.[27] This could be ascribed to more $CD9^-$ patients being stratified into the high-risk group due to inadequate Pred responses to receive intensive multiagent chemotherapy. Thus, the negative impact of GC resistance might have been overcome by other subsequent chemotherapeutic agents. Notably, CD9 also strongly predicted poor Pred responses in patients with unclassified BCP-ALL subtypes, as limited by our cytogenetics detection panel. With advances in deep genomic profiling,[46] it will be important to identify the exact molecular BCP-ALL subtypes that are specifically influenced by CD9 through a larger patient cohort. In contrast to BCP-ALL where $CD9^+$ cases predominated the patient population, the majority of T-ALL cases were $CD9^-$ as shown by our recent nationwide study.[28] Since GC resistance is a particular obstacle for T-ALL treatment,[47] it will be imperative to investigate whether GC responses are also shaped by CD9 in this leukemia type that could potentially inform new intervening strategies.

In pediatric ALL, mutations of the GC receptor *NR3C1* were rarely detected,[48,49] and evidence documenting the association between its expression and GC response appears conflicting.[50,51] Consistent with these findings, we observed ubiquitous mRNA and protein expression of NR3C1 in GC-sensitive $CD9^{high}$ and GC-resistant $CD9^{low}$ BCP-ALL cells. The same was also true for *NR3C1* isoforms and its mutational status. In addition, the phosphorylation of NR3C1 was robust, indicating that CD9 regulates GC

sensitivity through NR3C1 expression-, mutation- and activation-independent mechanisms. In line with the fact that tetraspanin family proteins typically act by forming microdomains with other partner proteins,[24] we reported for the first time that CD9 physically interacted with NR3C1 within the TEM. However, this interaction did not alter the nuclear translocation of NR3C1 and subsequent binding to GRE upon GC stimulation despite an elevated transcriptional program in the background of CD9. While the enhanced GC sensitivity in $CD9^{high}$ cells could potentially be explained by upregulation of proapoptotic genes such as BIM,[21] the mechanisms underlying how CD9 potentiates their transcription are still elusive and unlikely to be a direct consequence of altered NR3C1 activity. Given that NR3C1 is regulated by multiple signals (ligands, DNA-binding sequences, post-translational modifications and non-NR3C1 transcriptional regulatory factors),[52] one future direction is to map the whole spectrum of CD9 binding proteins within the TEM, coupled with a genome-scale knockout screen to functionally identify the partner(s) that are regulatory elements of GC-driven gene transcription.

Restoring GC sensitivity by enhancing CD9 expression, however, would be undesirable as it may at the same time increase leukemia aggressiveness.[27,28] Emerging studies suggest that GC resistance in BCP-ALL is mediated by constitutive activation of MAPK signaling.[17] In connection, the MEK inhibitor trametinib was recently approved for solid tumors with BRAF mutations,[53] and is now under clinal evaluation in combination with dexamethasone and chemotherapy for children with relapsed or refractory ALL or lymphoblastic lymphoma (NCT05658640). However, MEK or ERK phosphorylation varied extensively among patients and alone could not predict sensitivity to MEK inhibitors in multiple cancer types,[54,55] including BCP-ALL as shown in this study. Our data indeed showed that trametinib only exhibited strong synergism with GC in $CD9^{-}$ over $CD9^{+}$ BCP-ALL, suggesting that CD9 status could serve as a biomarker to identify patients who are most likely to benefit from this intervention. On the other hand, the lack of efficacy to the trametinib/GC combo in $CD9^{+}$ cases might originate from activation of parallel signaling pathways that cause intrinsic or adaptive resistance,[56,57] where GC-induced upregulation of *STAT5A* was evidenced only in the presence of CD9. The addition of ruxolitinib to $CD9^{+}$ lymphoblasts appeared to provide extra benefit on top of combinatorial trametinib/GC, suggesting a third drug targeting the JAK-STAT axis may be necessary to profit poor Pred responders with a $CD9^{+}$ phenotype.

References

1. Miranda-Filho A, Piñeros M, Ferlay J, Soerjomataram I, Monnereau A, Bray F. Epidemiological patterns of leukaemia in 184 countries: a population-based study. Lancet Haematol. 2018;5(1):e14-e24.

2. Hunger SP, Mullighan CG. Acute lymphoblastic leukemia in children. N Engl J Med. 2015;373(16):1541-1552.

3. Pui CH, Yang JJ, Hunger SP, et al. Childhood Acute Lymphoblastic Leukemia: Progress Through Collaboration. J Clin Oncol. 2015;33(27):2938-2948.

4. Tang J, Yu J, Cai J, et al. Prognostic factors for CNS control in children with acute lymphoblastic leukemia treated without cranial irradiation. Blood. 2021;138(4):331-343.

5. Bhojwani D, Pui CH. Relapsed childhood acute lymphoblastic leukaemia. Lancet Oncol. 2013;14(6):e205-e217.

6. Hunger SP, Raetz EA. How I treat relapsed acute lymphoblastic leukemia in the pediatric population. Blood. 2020;136(16):1803-1812.

7. Li CK, Chik KW, Ha SY, et al. Improved outcome of acute lymphoblastic leukaemia treated by delayed intensification in Hong Kong children: HKALL97 study. Hong Kong Med J. 2006;12(1):33-39.

8. Stary J, Zimmermann M, Campbell M, et al. Intensive chemotherapy for childhood acute lymphoblastic leukemia: Results of the randomized intercontinental trial ALL IC-BFM 2002. J Clin Oncol. 2014;32(3):174-184.

9. Cui L, Li ZG, Chai YH, et al. Outcome of children with newly diagnosed acute lymphoblastic leukemia treated with CCLG-ALL 2008: The first nation-wide prospective multicenter study in China. Am J Hematol. 2018;93(7):913-920.

10. Campbell M, Kiss C, Zimmermann M, et al. Childhood Acute Lymphoblastic Leukemia: Results of the Randomized Acute Lymphoblastic Leukemia Intercontinental-Berlin-Frankfurt-Münster 2009 Trial. J Clin Oncol. 2023;41(19):3499-3511.

11. Inaba H, Pui CH. Glucocorticoid use in acute lymphoblastic leukaemia. Lancet Oncol. 2010;11(11):1096-1106.

12. Schrappe M, Aricò M, Harbott J, et al. Philadelphia chromosome-positive (Ph+) childhood acute lymphoblastic leukemia: Good initial steroid response allows early prediction of a favorable treatment outcome. Blood. 1998;92(8):2730-2741.

13. Dördelmann M, Reiter A, Borkhardt A, et al. Prednisone response is the strongest predictor of treatment outcome in infant acute lymphoblastic leukemia. Blood. 1999;94(4):1209-1217.

14. Vandewalle J, Luypaert A, De Bosscher K, Libert C. Therapeutic Mechanisms of Glucocorticoids. Trends Endocrinol Metab. 2018;29(1):42-54.

15. Wandler AM, Huang BJ, Craig JW, et al. Loss of glucocorticoid receptor expression mediates in vivo dexamethasone resistance in T-cell acute lymphoblastic leukemia. Leukemia. 2020;34(8):2025-2037.

16. Mullighan CG, Zhang J, Kasper LH, et al. CREBBP mutations in relapsed acute lymphoblastic leukaemia. Nature. 2011;471(7337):235-239.

17. Jones CL, Gearheart CM, Fosmire S, et al. MAPK signaling cascades mediate distinct glucocorticoid resistance mechanisms in pediatric leukemia. Blood. 2015;126(19):2202-2212.

18. Real PJ, Tosello V, Palomero T, et al. γ-secretase inhibitors reverse glucocorticoid resistance in T cell acute lymphoblastic leukemia. Nat Med. 2009;15(1):50-58.

19. Xie M, Yang A, Ma J, et al. Akt2 mediates glucocorticoid resistance in lymphoid malignancies through FoxO3a/Bim axis and serves as a direct target for resistance reversal. Cell Death Dis. 2019;9(10):1013.

20. Poulard C, Kim HN, Fang M, et al. Relapse-associated AURKB blunts the glucocorticoid sensitivity of B cell acute lymphoblastic leukemia. Proc Natl Acad Sci U S A. 2019;116(8):3052-3061.

21. Jing D, Huang Y, Liu X, et al. Lymphocyte-specific chromatin accessibility pre-determines glucocorticoid resistance in acute lymphoblastic leukemia. Cancer Cell. 2018;34(6):906-921.

22. Olivas-Aguirre M, Torres-López L, Pottosin I, Dobrovinskaya O. Overcoming Glucocorticoid Resistance in Acute Lymphoblastic Leukemia: Repurposed Drugs Can Improve the Protocol. Front Oncol. 2021;11:617937.

23. Piovan E, Yu J, Tosello V, et al. Direct Reversal of Glucocorticoid Resistance by AKT Inhibition in Acute Lymphoblastic Leukemia. Cancer Cell. 2013;24(6):766-776.

24. Hemler ME. Tetraspanin functions and associated microdomains. Nat Rev Mol Cell Biol. 2005;6(10):801-811.

25. Zöller M. Tetraspanins: Push and pull in suppressing and promoting metastasis. Nat Rev Cancer. 2009;9(1):40-55.

26. Leung KT, Chan KY, Ng PC, et al. The tetraspanin CD9 regulates migration, adhesion, and homing of human cord blood CD34+ hematopoietic stem and progenitor cells. Blood. 2011;117(6):1840-1850.

27. Leung KT, Zhang C, Chan KY, et al. CD9 blockade suppresses disease progression of high-risk pediatric B-cell precursor acute lymphoblastic leukemia and enhances chemosensitivity. Leukemia. 2020;34(3):709-720.

28. Leung KT, Cai J, Liu Y, et al. Prognostic implications of CD9 in childhood acute lymphoblastic leukemia: insights from a nationwide multicenter study in China. Leukemia. 2024;38(2):250-257.

29. Chan KYY, Zhang C, Wong YTS, et al. R4 RGS proteins suppress engraftment of human hematopoietic stem/progenitor cells by modulating SDF-1/CXCR4 signaling. Blood Adv. 2021;5(21):4380-4392.

30. Lee SHR, Yang W, Gocho Y, et al. Pharmacotypes across the genomic landscape of pediatric acute lymphoblastic leukemia and impact on treatment response. Nat Med. 2023;29(1):170-179.

31. Wang H, Chan KYY, Cheng CK, et al. Pharmacogenomic profiling of pediatric acute myeloid leukemia to identify therapeutic vulnerabilities and inform functional precision medicine. Blood Cancer Discov. 2022;3(6):516-535.

32. Bliss CI. The Toxicity of Poisons Applied Jointly. Ann Appl Biol. 1939;26(3):585-615.

33. Liu T, Rao J, Hu W, et al. Distinct genomic landscape of Chinese pediatric acute myeloid leukemia impacts clinical risk classification. Nat Commun. 2022;13(1):1640.

34. Zhang C, Zhang B, Lin L-L, Zhao S. Evaluation and comparison of computational tools for RNA-seq isoform quantification. BMC Genomics. 2017;18(1):583.

35. Verbeke D, Demeyer S, Prieto C, et al. The XPO1 Inhibitor KPT-8602 Synergizes with Dexamethasone in Acute Lymphoblastic Leukemia. Clin Cancer Res. 2020;26(21):5747-5758.

36. Kerstjens M, Pinhancos SS, Castro PG, et al. Trametinib inhibits RAS-mutant MLL-rearranged acute lymphoblastic leukemia at specific niche sites and reduces ERK phosphorylation in vivo. Haematologica. 2018;103(4):e147-e150.

37. Haarman EG, Kaspers GJL, Pieters R, Rottier MMA, Veerman AJP. Glucocorticoid receptor alpha, beta and gamma expression vs in vitro glucocorticod resistance in childhood leukemia. Leukemia. 2004;18(3):530-537.

38. Liu H, Li Z, Qiu F, et al. Association Between NR3C1 Mutations and Glucocorticoid Resistance in Children With Acute Lymphoblastic Leukemia. Front Pharmacol. 2021;12:634956.

39. Wasim M, Carlet M, Mansha M, et al. PLZF/ZBTB16, a glucocorticoid response gene in acute lymphoblastic leukemia, interferes with glucocorticoid-induced apoptosis. J Steroid Biochem Mol Biol. 2010;120(4-5):218-227.

40. Riccardi C, Cifone MG, Migliorati G. Glucocorticoid hormone-induced modulation of gene expression and regulation of T-cell death: role of GITR and GILZ, two dexamethasone-induced genes. Cell Death Differ. 1999;6(12):1182-1189.

41. Chan LN, Murakami MA, Robinson ME, et al. Signalling input from divergent pathways subverts B cell transformation. Nature. 2020;583(7818):845-851.

42. Hu X, Xuan H, Du H, Jiang H, Huang J. Down-regulation of CD9 by methylation decreased bortezomib sensitivity in multiple myeloma. PloS One. 2014;9(5):e95765.

43. Ullah M, Akbar A, Ng NN, Concepcion W, Thakor AS. Mesenchymal stem cells confer chemoresistance in breast cancer via a CD9 dependent mechanism. Oncotarget. 2019;10(37):3435-3450.

44. Kohmo S, Kijima T, Otani Y, et al. Cell Surface Tetraspanin CD9 Mediates Chemoresistance in Small Cell Lung Cancer. Cancer Res. 2010;70(20):8025-8035.

45. Maloney KW, Devidas M, Wang C, et al. Outcome in children with standard-risk B-cell acute lymphoblastic leukemia: results of children's oncology group trial AALL0331. J Clin Oncol. 2020;38(6):602-612.

46. Brady SW, Roberts KG, Gu Z, et al. The genomic landscape of pediatric acute lymphoblastic leukemia. Nat Genet. 2022;54(9):1376-1389.

47. De Smedt R, Morscio J, Goossens S, Van Vlierberghe P. Targeting steroid resistance in T-cell acute lymphoblastic leukemia. Blood Rev. 2019;38:100591.

48. Ding LW, Sun QY, Tan KT, et al. Mutational landscape of pediatric acute lymphoblastic leukemia. Cancer Res. 2017;77(2):390-400.

49. Oshima K, Khiabanian H, da Silva-Almeida AC, et al. Mutational landscape, clonal evolution patterns, and role of RAS mutations in relapsed acute lymphoblastic leukemia. Proc Natl Acad Sci. 2016;113(40):11306-11311.

50. Lauten M, Cario G, Asgedom G, Welte K, Schrappe M. Protein expression of the glucocorticoid receptor in childhood acute lymphoblastic leukemia. Haematologica. 2003;88(11):1253-1258.

51. Koga Y, Matsuzaki A, Suminoe A, Hattori H, Kanemitsu S, Hara T. Differential mRNA expression of glucocorticoid receptor α and β is associated with glucocorticoid sensitivity of acute lymphoblastic leukemia in children. Pediatr Blood Cancer. 2005;45(2):121-127.

52. Weikum ER, Knuesel MT, Ortlund EA, Yamamoto KR. Glucocorticoid receptor control of transcription: precision and plasticity via allostery. Nat Rev Mol Cell Biol. 2017;18(3):159-174.

53. Dummer R, Long GV, Robert C, et al. Randomized Phase III Trial Evaluating Spartalizumab Plus Dabrafenib and Trametinib for BRAF V600-Mutant Unresectable or Metastatic Melanoma. J Clin Oncol. 2022;40(13):1428-1438.

54. Rožanc J, Sakellaropoulos T, Antoranz A, et al. Phosphoprotein patterns predict trametinib responsiveness and optimal trametinib sensitisation strategies in melanoma. Cell Death Differ. 2019;26(8):1365-1378.

55. Wagle M-C, Kirouac D, Klijn C, et al. A transcriptional MAPK Pathway Activity Score (MPAS) is a clinically relevant biomarker in multiple cancer types. NPJ Precis Oncol. 2018;2(1):7.

56. Perna D, Karreth FA, Rust AG, et al. BRAF inhibitor resistance mediated by the AKT pathway in an oncogenic BRAF mouse melanoma model. Proc Natl Acad Sci U S A. 2015;112(6):E536-545.

57. Vultur A, Villanueva J, Krepler C, et al. MEK inhibition affects STAT3 signaling and invasion in human melanoma cell lines. Oncogene. 2014;33(14):1850-1861.

Table 1. Association of CD9 with prednisone response in pediatric B-cell precursor acute lymphoblastic leukemia

		All patients (n =182)		$CD9^+$ patients (n=146)		$CD9^-$ patients (n=36)		$CD9^+$ *vs.* $CD9^-$
Prednisone response		**Good**	**Poor**	**Good**	**Poor**	**Good**	**Poor**	***P* value**
Whole cohort								
	No.	166	16	137	9	29	7	**0.020**
	%	91.2	8.8	93.8	6.2	80.6	19.4	
Age (years)								
<1	**No.**	13	3	11	3	2	0	>0.999
	%	81.3	18.7	78.6	21.4	100	0	
1-9.9	**No.**	125	9	100	5	25	4	0.101
	%	93.3	6.7	95.2	4.8	86.2	13.8	
≥10	**No.**	28	4	26	1	2	3	**0.008**
	%	87.5	12.5	96.3	3.7	40.0	60.0	
Sex								
Male	**No.**	102	11	84	6	18	5	**0.045**
	%	90.3	9.7	93.3	6.7	78.3	21.7	
Female	**No.**	64	5	53	3	11	2	0.235
	%	92.8	7.2	94.6	5.4	84.6	15.4	
White cell count ($\times 10^9$/L)								
<50	**No.**	130	4	104	3	26	1	>0.999
	%	97.0	3.0	97.2	2.8	96.3	3.7	
≥50	**No.**	36	12	33	6	3	6	**0.004**
	%	75.0	25.0	84.6	15.4	33.3	66.7	
Cytogenetics								
Hyperdiploidy*****	**No.**	29	1	29	1	0	0	-
	%	96.7	3.3	96.7	3.3	0	0	
BCR-ABL1	**No.**	7	4	7	1	0	3	**0.024**
	%	63.6	36.4	87.5	12.5	0	100	
*ETV6-RUNX1******	**No.**	35	0	18	0	17	0	-
	%	100	0	100	0	100	0	
KMT2A-rearranged	**No.**	12	2	9	2	3	0	>0.999
	%	85.7	14.3	81.8	18.2	100	0	
*TCF3-PBX1******	**No.**	9	1	9	1	0	0	-
	%	90.0	10.0	90.0	10.0	0	0	
B-others	**No.**	74	8	65	4	9	4	**0.019**
	%	90.2	9.8	94.2	5.8	69.2	30.8	
Risk group								
Standard risk	**No.**	73	1	57	1	16	0	>0.999
	%	98.6	1.4	98.3	1.7	100	0	
Intermediate risk	**No.**	77	2	68	1	9	1	0.282
	%	97.5	2.5	98.6	1.4	90.0	10.0	
High risk	**No.**	16	13	12	7	4	6	0.270
	%	55.2	44.8	63.2	36.8	40.0	60.0	

Statistics: Fisher's exact test.

*****No statistics are computed because CD9 or prednisone response is a constant.

Figure Legends

Figure 1. Drug sensitivity profiling reveals preferential resistance of CD9^{low} B-cell precursor acute lymphoblastic leukemia cells to glucocorticoids. (A, left) Heatmap showing the responses of B-cell precursor acute lymphoblastic leukemia cell lines to standard therapeutic agents. The color scale delineates the $\log_{10}$ IC50 range. Cluster A, drugs without differential activities between CD9^{high} and CD9^{low} cells. Cluster B, drugs with differential activities between CD9^{high} and CD9^{low} cells. (A, right) Flow histograms showing cell surface CD9 expression on individual B-cell precursor acute lymphoblastic leukemia cell lines. The percentages of CD9^{+} populations and MFI (numbers in bracket) are indicated. The mean CD9 expression is shown on the top and was used define CD9 status. (B) *Ex vivo* responses of CD9^{-} (n=6) and CD9^{+} (n=12) B-cell precursor acute lymphoblastic leukemia samples to Pred or Dex. Cytogenetic features of individual samples are annotated. Statistics: 2-tailed, unpaired Student's *t*-test. *****P<0.05. (C) Representative flow cytometry plots showing the levels of apoptotic lymphoblasts of CD9^{+} and CD9^{-} cases after treatment with 100 μM Pred or Dex for 96 hours in MSC cocultures. Abbreviations: Ara-C, cytarabine; DNR, daunorubicin; VCR, vincristine; MTX, methotrexate; Pred, prednisolone; Dex, dexamethasone; IC50, half-maximal inhibitory concentration.

Figure 2. CD9 is functionally linked to glucocorticoid sensitivity. (A) Schematic diagram of lentiviral vectors for CD9 overexpression. SFFV, spleen focus-forming virus U3 promoter; E2A, a self-cleavage site derived from equine rhinitis A virus; GFP, green fluorescence protein. Shown are representative flow cytometry plots depicting the expression of GFP and CD9 in transduced SEM cells after puromycin selection. (B) Differential sensitivity of control SEM-GFP and experimental SEM-CD9-GFP cells to glucocorticoids (n=8-9). (C) Responses of transduced SEM cells to other chemotherapeutic agents (n=6-8). (D) Representative flow cytometry plots showing the expression of GFP and CD9 in stably transduced KOPN-8 cells, and their sensitivity to glucocorticoids (n=7-10). (E) Schematic diagram of lentiviral vectors for CD9 knockout. U6, RNA polymerase III promoter; sg, single-guide RNA; Cas9, CRISPR associated protein 9. Shown are representative flow cytometry plots depicting the expression of GFP and CD9 in transduced 697 cells after FACS sorting. (F) Differential sensitivity of control 697-CTsg-GFP and

experimental 697-CD9sg-GFP cells to glucocorticoids (n=10). Statistics: two-tailed, paired Student's *t*-test. *****P<0.05, ******P<0.01, *******P<0.001, N.S., not significant.

Figure 3. CD9 binds to NR3C1 but does not affect its expression, phosphorylation and nuclear translocation. (A) Expression of NR3C1 in $CD9^+$ (n=12) or $CD9^-$ (n=6) B-cell precursor acute lymphoblastic leukemia samples as revealed by Western blotting, with GAPDH as the internal control. (B) *NR3C1* and *CD9* mRNA expression in patient samples relative to *GAPDH* and their correlation. (C) Phosphorylation status of NR3C1 in SEM-GFP and SEM-CD9-GFP cells after an 8-hour exposure to DMSO, Pred (50 μM) or Dex (1 μM). (D) NR3C1 protein level in fractionated lysates of SEM-GFP and SEM-CD9-GFP cells with or without exposure to glucocorticoids (Pred, 50 μM; Dex, 1 μM for 8 hours). NR3C1/GAPDH intensity ratios for the cytoplasmic fraction or NR3C1/H3 ratios for the nuclear fraction are shown. (E) Lysates from SEM-GFP and SEM-CD9-GFP after glucocorticoid treatments (Pred, 50 μM; Dex, 1 μM for 8 hours) were immunoprecipitated with control IgG_{2b} or anti-CD9, and probed with antibodies against NR3C1, CD9 or GAPDH after electrophoresis. The levels of co-precipitated NR3C1 normalized to lysate input in respective treatments are shown. All presented images are representative of at least 3 independent experiments. Statistics: (A) Fisher's exact test; (B, left) two-tailed, unpaired Student's *t*-test; (B, right) Spearman's correlation. ******P<0.01, N.S., not significant.

Figure 4. CD9 potentiates the expression of glucocorticoid-responsive genes. SEM-GFP and SEM-CD9-GFP cells were exposed to Dex (1 μM) for 8 hours and subjected to RNA-seq, qRT-PCR and ChIP-seq. (A) Volcano plots showing the DEGs in Dex-treated SEM-GFP (n=82) and SEM-CD9-GFP cells (n=110) identified by RNA-seq. Suppressed DEGs are indicated in blue, and augmented DEGs in red. (B) Venn diagram showing the number of overlapping and exclusive DEGs in SEM-GFP and SEM-CD9-GFP cells induced by Dex. (C) qRT-PCR validation of selected DEGs (n=4-7). The indicated values are the fold induction by Dex over DMSO. Statistics: two-tailed, paired Student's *t*-test comparing (i) the changes in gene expression upon Dex treatment of SEM-GFP (blue) or SEM-CD9-GFP cells (red), *****P<0.05, ******P<0.01, *******P<0.001; and (ii) the magnitudes of glucocorticoid-mediated gene induction between SEM-GFP and SEM-CD9-GFP cells (blue *vs.* red), $^{\#}P$<0.05, $^{\#\#}P$<0.01. (D) Individual NR3C1 ChIP-seq tracks for selected

glucocorticoid-responsive genes.

Figure 5. MEK inhibition restores the susceptibility of CD9^{low} cells to glucocorticoids. (A) NSG mice were infused with luciferase-expressing CD9^{low} SEM or CD9^{high} BV-173 cells (1×10^6/mouse), and randomized to receive daily treatment of vehicle control, Dex (5 mg/kg by intraperitoneal injection), trametinib (5 mg/kg by oral gavage) or their combination for 2 weeks (5 days on, 2 days off) starting on day 3 after leukemic cell infusion (4-5 mice/group). (Left) Systematic leukemic load was monitored by bioluminescence imaging when animals in the vehicle groups reached humane endpoints (day 33 for SEM; day 28 for BV-173). (Right) Concurrent enumeration of leukemic blasts in the bone marrow by flow cytometry. Blasts were defined as human CD45$^+$CD19$^+$ cells. (B) Mode of trametinib/Dex interactions in CD9$^+$ (n=5) and CD9$^-$ (n=3) samples. The Bliss scores of individual samples are indicated, with red bars indicating drug synergy and green bars representing drug antagonism. Asterisks denote samples chosen for JAK-STAT inhibition experiments. (C) *STAT5A* expression in SEM-GFP and SEM-CD9-GFP cells (n=6). The indicated values are the fold induction by Dex over DMSO. (D) Lymphoblasts from CD9$^+$ cases (n=4) were treated with single agent ruxolitinib (0.1 nM), trametinib (10nM), Dex (1-10 nM) or their combinations for 96 hours in MSC cocultures. Shown are the mean percentage of viable cells relative to DMSO controls. Statistics: (A) two-tailed, unpaired Student's *t*-test; (C,D) two-tailed, paired Student's *t*-test. *****P<0.05, ******P<0.01, $^{\#}P$<0.05, N.S., not significant.

Figure 1

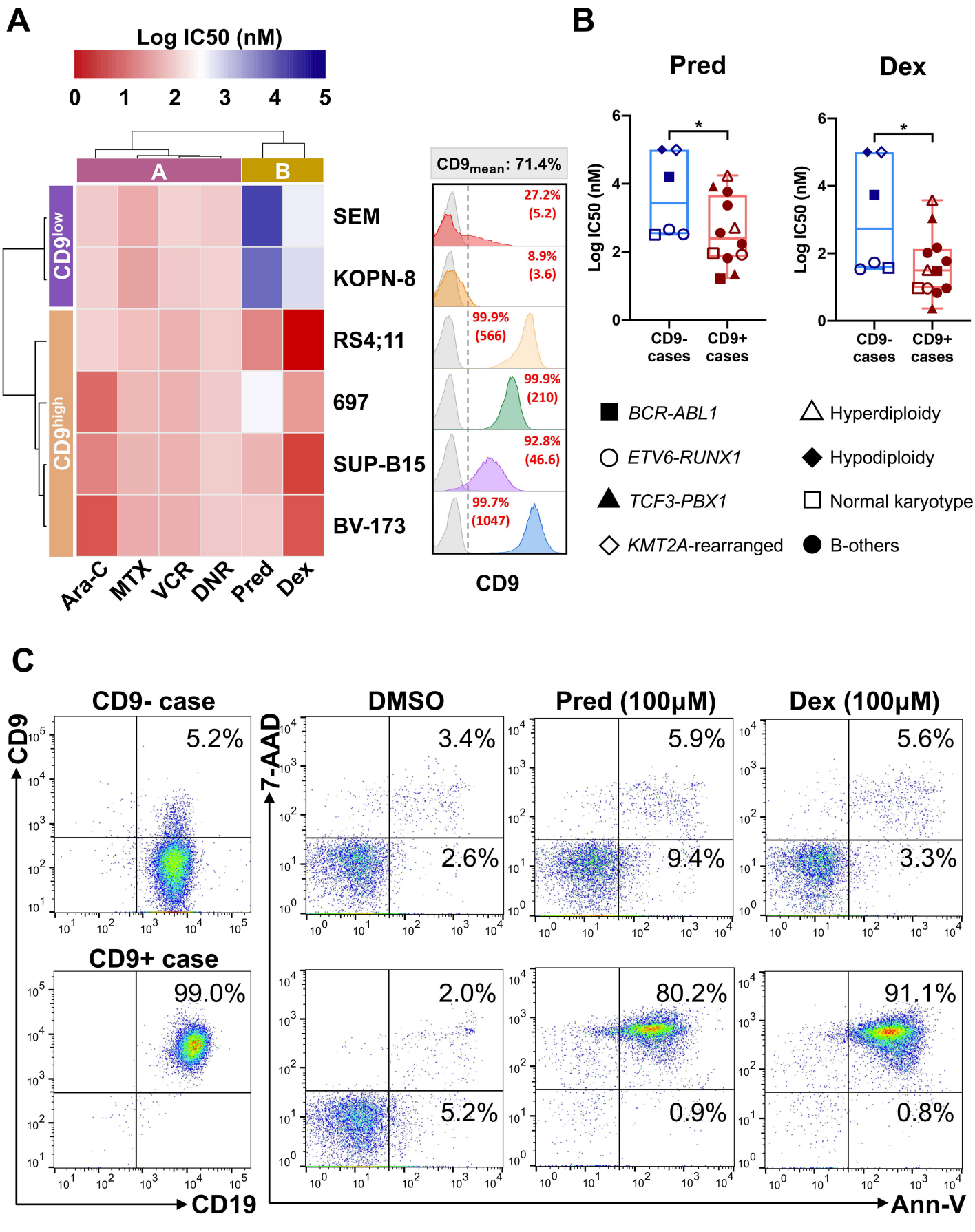
A
Log IC50 (nM)
0 1 2 3 4 5
A
B
CD9low
CD9high
SEM
KOPN-8
RS4;11
697
SUP-B15
BV-173
Ara-C
MTX
VCR
DNR
Pred
Dex
CD9mean: 71.4%
27.2% (5.2)
8.9% (3.6)
99.9% (566)
99.9% (210)
92.8% (46.6)
99.7% (1047)
CD9
B
Pred
Dex
Log IC50 (nM)
CD9- cases
CD9+ cases
*
BCR-ABL1
ETV6-RUNX1
TCF3-PBX1
KMT2A-rearranged
Hyperdiploidy
Hypodiploidy
Normal karyotype
B-others
C
CD9- case
CD9+ case
DMSO
Pred (100μM)
Dex (100μM)
CD9
CD19
7-AAD
Ann-V
5.2%
3.4%
2.6%
5.9%
9.4%
5.6%
3.3%
99.0%
2.0%
5.2%
80.2%
0.9%
91.1%
0.8%

Figure 2

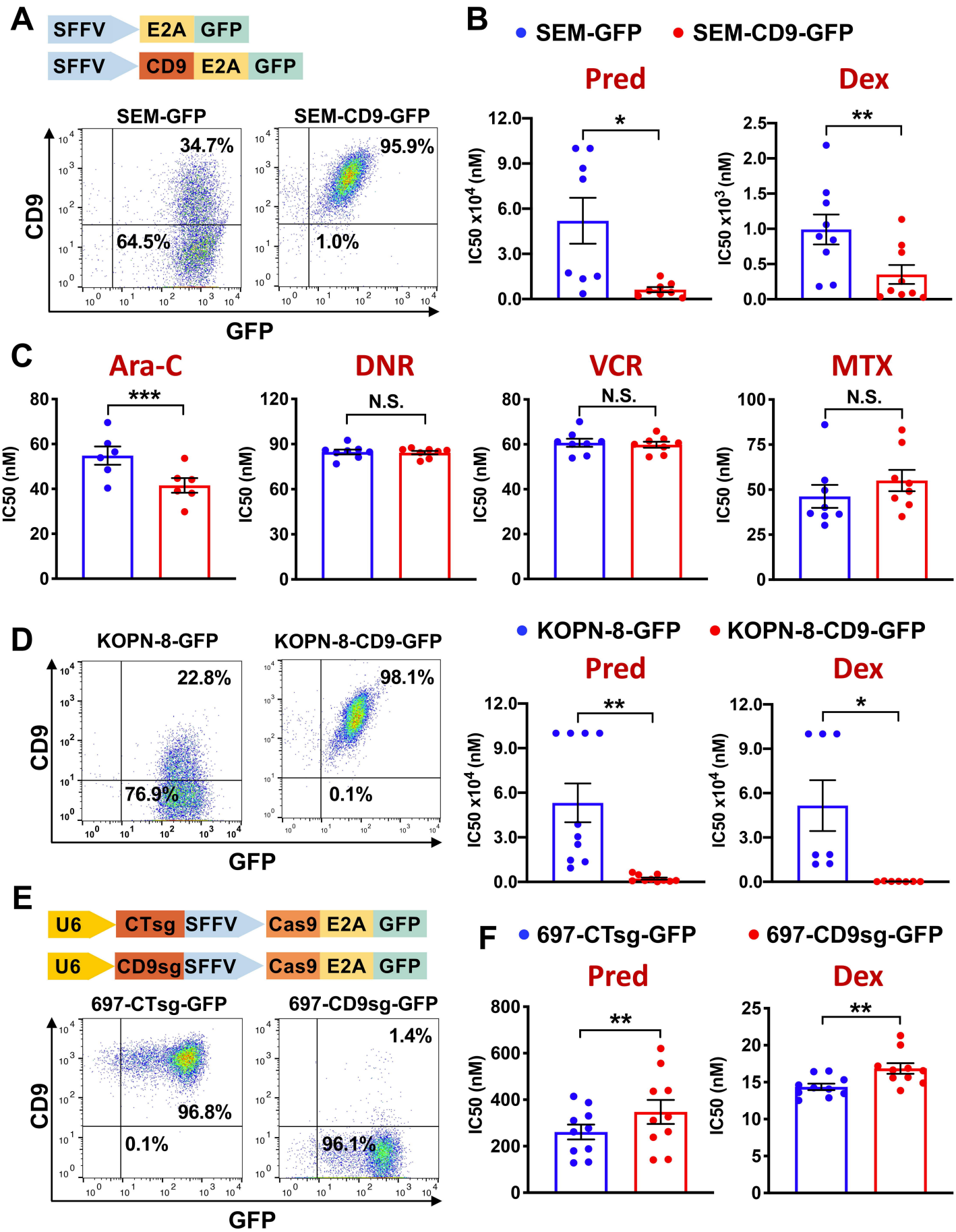
A
SFFV E2A GFP
SFFV CD9 E2A GFP
SEM-GFP
SEM-CD9-GFP
34.7%
64.5%
95.9%
1.0%
CD9
GFP
B
SEM-GFP
SEM-CD9-GFP
Pred
Dex
IC50 x10^4 (nM)
IC50 x10^3 (nM)
*
**
C
Ara-C
DNR
VCR
MTX
IC50 (nM)
***
N.S.
D
KOPN-8-GFP
KOPN-8-CD9-GFP
22.8%
76.9%
98.1%
0.1%
E
U6 CTsg SFFV Cas9 E2A GFP
U6 CD9sg SFFV Cas9 E2A GFP
697-CTsg-GFP
697-CD9sg-GFP
96.8%
0.1%
1.4%
96.1%
F
697-CTsg-GFP
697-CD9sg-GFP

Figure 3

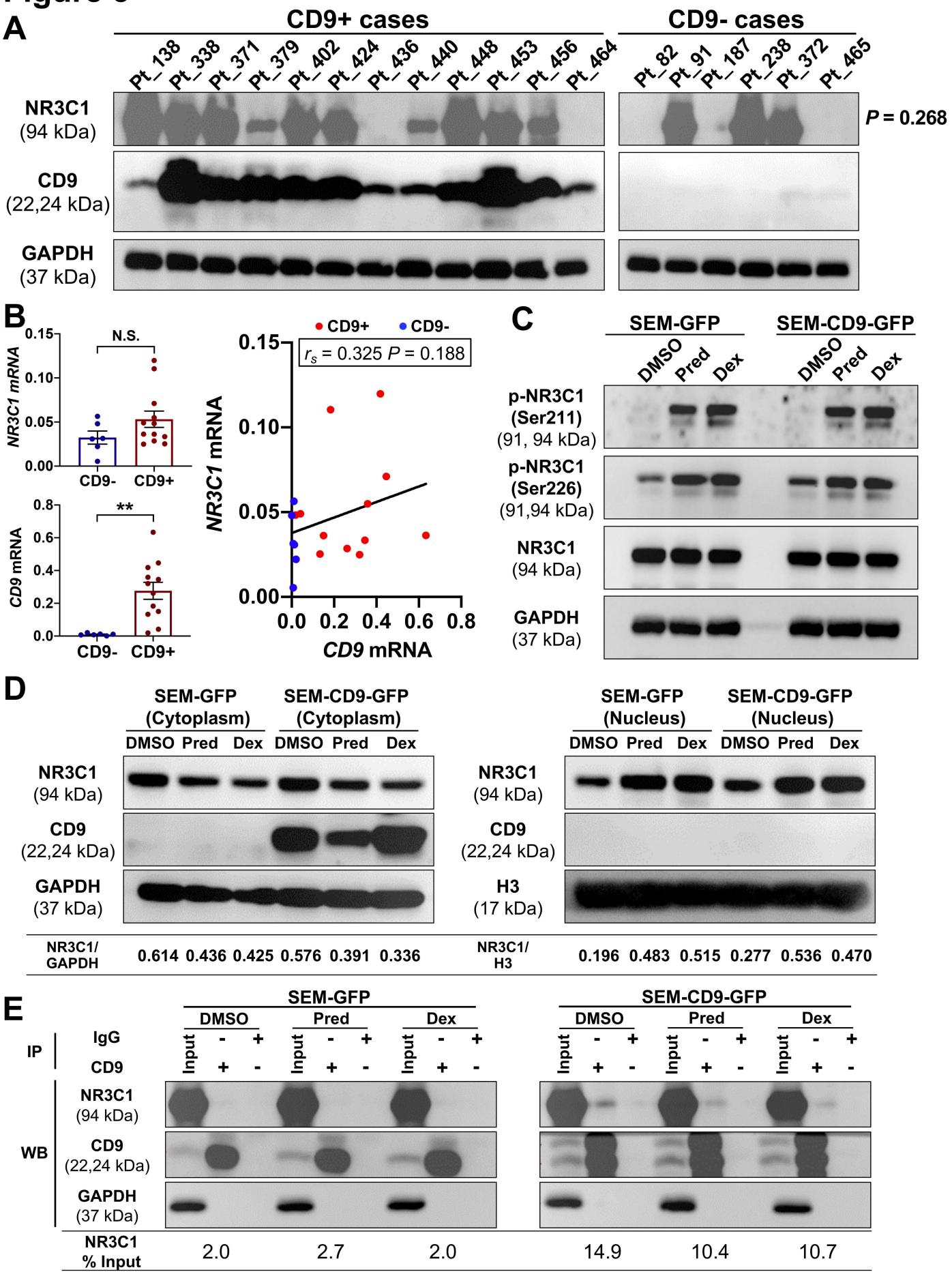
A
CD9+ cases
CD9- cases
Pt_138
Pt_338
Pt_371
Pt_379
Pt_402
Pt_424
Pt_436
Pt_440
Pt_448
Pt_453
Pt_456
Pt_464
Pt_82
Pt_91
Pt_187
Pt_238
Pt_372
Pt_465
NR3C1 (94 kDa)
CD9 (22,24 kDa)
GAPDH (37 kDa)
P = 0.268
B
N.S.
NR3C1 mRNA
CD9-
CD9+
**
CD9 mRNA
CD9+
CD9-
r_s = 0.325 P = 0.188
NR3C1 mRNA
CD9 mRNA
C
SEM-GFP
SEM-CD9-GFP
DMSO
Pred
Dex
p-NR3C1 (Ser211) (91, 94 kDa)
p-NR3C1 (Ser226) (91,94 kDa)
NR3C1 (94 kDa)
GAPDH (37 kDa)
D
SEM-GFP (Cytoplasm)
SEM-CD9-GFP (Cytoplasm)
SEM-GFP (Nucleus)
SEM-CD9-GFP (Nucleus)
DMSO Pred Dex DMSO Pred Dex
NR3C1 (94 kDa)
CD9 (22,24 kDa)
GAPDH (37 kDa)
H3 (17 kDa)
NR3C1/ GAPDH
0.614 0.436 0.425 0.576 0.391 0.336
NR3C1/ H3
0.196 0.483 0.515 0.277 0.536 0.470
E
SEM-GFP
SEM-CD9-GFP
DMSO
Pred
Dex
IP
IgG
CD9
Input
WB
NR3C1 (94 kDa)
CD9 (22,24 kDa)
GAPDH (37 kDa)
NR3C1 % Input
2.0 2.7 2.0 14.9 10.4 10.7

Figure 4

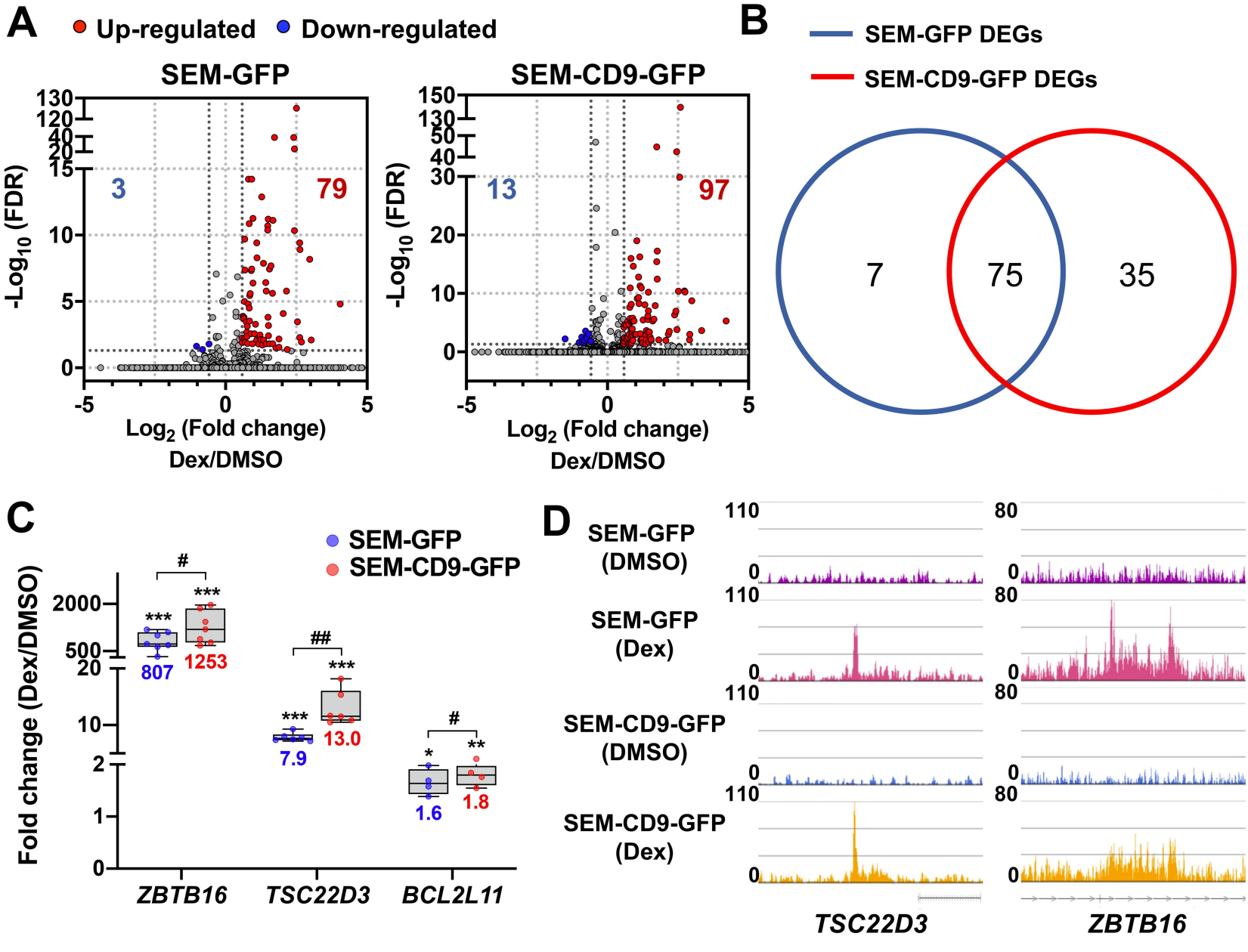
A
Up-regulated
Down-regulated
SEM-GFP
SEM-CD9-GFP
-Log10 (FDR)
Log2 (Fold change)
Dex/DMSO
3
79
13
97
B
SEM-GFP DEGs
SEM-CD9-GFP DEGs
7
75
35
C
SEM-GFP
SEM-CD9-GFP
Fold change (Dex/DMSO)
807
1253
7.9
13.0
1.6
1.8
ZBTB16
TSC22D3
BCL2L11
D
SEM-GFP (DMSO)
SEM-GFP (Dex)
SEM-CD9-GFP (DMSO)
SEM-CD9-GFP (Dex)
TSC22D3
ZBTB16

Figure 5

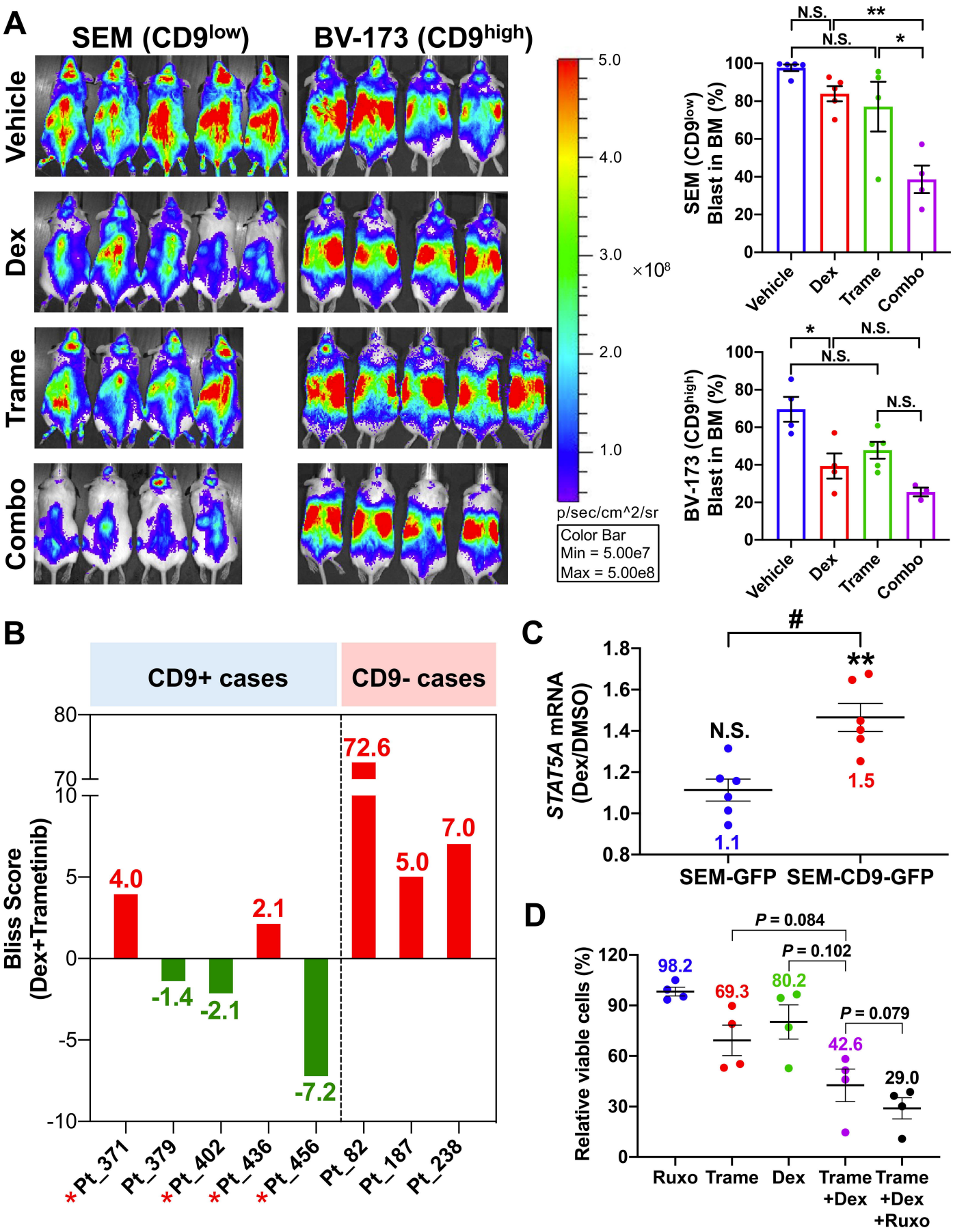
A
SEM (CD9low)
BV-173 (CD9high)
Vehicle
Dex
Trame
Combo
5.0
4.0
3.0
×10^8
2.0
1.0
p/sec/cm^2/sr
Color Bar
Min = 5.00e7
Max = 5.00e8
N.S.
**
N.S.
*
SEM (CD9low) Blast in BM (%)
Vehicle
Dex
Trame
Combo
*
N.S.
N.S.
N.S.
BV-173 (CD9high) Blast in BM (%)
B
CD9+ cases
CD9- cases
Bliss Score (Dex+Trametinib)
4.0
-1.4
-2.1
2.1
-7.2
72.6
5.0
7.0
*Pt_371
Pt_379
*Pt_402
*Pt_436
*Pt_456
Pt_82
Pt_187
Pt_238
C
#
**
N.S.
STAT5A mRNA (Dex/DMSO)
1.1
1.5
SEM-GFP
SEM-CD9-GFP
D
P = 0.084
P = 0.102
P = 0.079
Relative viable cells (%)
98.2
69.3
80.2
42.6
29.0
Ruxo
Trame
Dex
Trame +Dex
Trame +Dex +Ruxo

Supplemental Information for Zhang et al

"CD9 shapes glucocorticoid sensitivity in pediatric B-cell precursor acute lymphoblastic leukemia"

Supplemental Methods

Cells and CD9 characterization

BCP-ALL cell lines 697, BV-173, KOPN-8, RS4;11 and SEM (DSMZ, Braunchweig, Germany) as well as SUP-B15 (ATCC, Manassas, VA, USA) were maintained in RPMI-1640 medium (Life Technologies, Waltham, MA, USA) supplemented with 10% fetal bovine serum (Life Technologies). The cell surface CD9 expression was characterized by CD9-PE antibody (clone M-L13; BD Biosciences, San Jose, CA, USA). Primary lymphoblasts were recovered from cryopreserved, diagnostic bone marrow samples of pediatric BCP-ALL patients by density gradient centrifugation using Ficoll-Paque Plus (GE Healthcare, Chicago, IL, USA) and delineated for purity with fluorochrome-conjugated antibodies: CD9-PE, CD19-BV605 (clone HIB19; BD Biosciences), CD34-PE-Cy7 (clone 8G12; BD Biosciences), and CD45-APC (clone J.33; Beckman Coulter, Brea, CA, USA). Cell surface CD9 expression on $CD45^{dim/-}CD34^{+/-}CD19^{+}$ blasts was determined by flow cytometry (LSRFortessa, BD Biosciences), with negative populations defined by respective isotype controls. All FACS data were analyzed using FlowJo software v10.4 (TreeStar, Ashland, OR, USA).

Drug sensitivity assay

BCP-ALL cell lines (5×10^4-1×10^5) were seeded into 96-well plates (Corning, NY, USA) and treated with DMSO control or 0.1 nM-100 μM of Pred, Dex, Ara-C, DNR, VCR, or MTX (Selleckchem, Houston, TX, USA) for 72 hours. In some experiments, leukemic cells were treated with Pred or Dex in combination with 0.1-100 μM of trametinib (MedChemExpress, Monmouth Junction, NJ, USA). Cell proliferation was measured using the CellTiter MTS solution according to the manufacturer's instructions (Promega, Madison, WI, USA).

Primary lymphoblasts (1.6×10^5) were seeded onto GFP-expressing, hTERT-immortalized mesenchymal stem cells (MSCs, 1×10^4) and treated with DMSO or 0.1 nM-100 μM of Pred or Dex for 96 hours.[1] On some occasions, lymphoblasts were concomitantly treated with trametinib and/or ruxolitinib (MedChemExpress) at the indicated concentrations. Cells were recovered by 0.25% trypsin (Gibco, Grand Island, NY, USA). Leukemic cells were identified with CD19-BV421 (clone HIB19; BD Biosciences). Annexin V^-/7-AAD^- viable cells were recognized using the Apoptosis Detection Kit (BD Biosciences) by flow cytometry. The percentage of viable cells was normalized against DMSO

controls with outliers removed before curve fitting. The half-maximal inhibitory concentrations (IC50s) were calculated from the dose-response curves by nonlinear regression using the GraphPad Prism software (GraphPad, San Diego, CA, USA). The IC50 values were designated as the highest dose (*i.e.* 100 μM) whenever the cell viability remained >50% across the entire dose range.[2] Hierarchical clustering was performed using the Euclidean distance metric and Ward's minimum variance method for linkage[3] to generate drug clusters (clusters A and B) with the Pheatmap package in R v3.4.1 (http://cran.r-project.org/web/packages/pheatmap/index.html). The Bliss score indicating synergy of drug combinations was calculated using SynergyFinder.[4]

Patient cohort

Children with BCP-ALL were recruited from three clinical studies conducted in the Prince of Wales Hospital, Hong Kong between 1997 and 2015: HKALL 97,[5] IC-BFM ALL 2002[6] and CCLG 2008.[7] These clinical studies commonly adopted a Berlin-Frankfurt-Münster (BFM)-based treatment protocol, with a prephase of 7-day oral Pred at 60 mg/m^2 before the commencement of multiagent chemotherapy. Baseline demographic data, clinical parameters and pathologic variables of the recruited patients were retrieved from the medical records. Specimens were collected with informed written consent following the Declaration of Helsinki. The study was approved by the Joint Chinese University of Hong Kong – New Territories East Cluster Clinical Research Ethics Committee.

Lentiviral vectors and transduction

For gain-of-function studies, the human CD9 full-length open reading frame (Open Biosystems, Huntsville, AL, USA) was inserted into the pRSC-SFFV-E2A-GFP-Wpre lentiviral backbone by PCR cloning and verified by Sanger sequencing (ABI 3130 Genetic Analyzer, Applied Biosystem, Foster City, CA, USA). For loss-of-function studies, a single-guide RNA (sgRNA) targeting human CD9 (GGGATATTCCCACAAGGATG) or a non-targeting sgRNA (GCACTCACATCGCTACATCA) was inserted into the pRSC-U6-SFFV-Cas9-E2A-GFP-Wpre lentiviral backbone. VSVG-pseudotyped vectors were packaged in 293T cells (ATCC), with functional viral titers determined by transduction of HT1080 cells (ATCC) followed by flow cytometry analysis.[8] CD9^{low} cells were transduced with control GFP-only or CD9-GFP lentiviral particles, whereas CD9^{high} cells were transduced with control sgRNA-GFP or CD9 sgRNA-GFP lentiviral particles at a multiplicity of infection of 4-8 for 48 hours

in non-TC-treated plates precoated with RetroNectin (50 μg/mL; Takara Bio Inc., Shiga, Japan). The transduction efficiency was determined by quantification of GFP^+ cells coupled with CD9-APC antibody staining (clone M-L13; BD Biosciences). Stable cell lines were generated by selection with puromycin (1 μg/mL; Life Technologies) or cell sorting (FACSAria Fusion, BD Biosciences).

Western blotting and co-immunoprecipitation

BCP-ALL cells (5×10^6), with or without GC treatments, were lysed in RIPA buffer (Sigma-Aldrich, St. Louis, MO, USA) supplemented with protease inhibitor cocktails (Roche Diagnostics, Indianapolis, IN, USA) to obtain total cell lysates. On some occasions, subcellular components were recovered with a Cell Fractionation Kit following the manufacturer's protocols (Cell Signaling Technology, Danvers, MA, USA). Protein concentrations were measured with the DC Protein Assay Kit (Bio-Rad, Hercules, CA, USA). Lysates (30-50 μg) were separated by SDS-PAGE and probed with antibodies against CD9 (clone D8O1A), phospho-NR3C1 (Ser211, polyclonal), phospho-NR3C1 (Ser226, clone D9D3V), NR3C1 (clone D6H2L), phospho-MEK1/2 (Ser217/221, clone 41G9), MEK1/2 (clone 47E6), phospho-ERK1/2 (Thr202/Tyr204, clone D13.14.4E) or ERK1/2 (clone 137F5), with GAPDH (clone 14C10) or histone H3 (clone D1H2) as loading controls where appropriate. All primary antibodies were from Cell Signaling Technology and used at a fixed dilution of 1:1000. The reactions were developed with peroxidase-conjugated goat-anti-rabbit secondary antibodies (1:5000) followed by detection with SignalFire Plus ECL Reagent or SiganlFire Elite ECL Reagent (Cell Signaling Technology). Chemiluminescence snapshots were captured on the Alliance Q9 Advanced Imager (UVItec, Cambridge, UK).

For co-immunoprecipitation assays, BCP-ALL cells (9×10^8) treated with GCs were lysed in 1% Brij97 buffer (Sigma-Aldrich). Cell lysates (900 μg) were immunoprecipitated with 10 μg isotype control IgG_{2b} (clone 20016; R&D Systems, Minneapolis, MN, USA) or CD9 antibody (clone MM2/57; Millipore, Billerica, MA, USA) at 4°C overnight. Immune complexes were captured with protein A/G agarose (Pierce, Waltham, MA, USA) and separated by SDS-PAGE. Immunoblots were then probed with antibodies against CD9 (clone D8O1A, Cell Signaling Technology), NR3C1 (clone D6H2L, Cell Signaling Technology), CD81 (clone D3N2D, Cell Signaling Technology) or EWI-2 (clone: 2587A, R&D systems), as described.

RNA sequencing

Total RNA was extracted from patient samples or Dex-treated BCP-ALL cells using TRIzol reagent (Life Technologies) and RNeasy Micro Kit (Qiagen, Hilden, Germany). After ribosomal RNA removal (Ribo-zero, Epicenter, Madison, WI, USA), cDNA libraries were generated by the NEBNext Ultra Directional RNA Library Prep Kit (New England BioLabs, Ipswich, MA, USA) and sequenced on a NovaSeq 6000 platform (Illumina, San Diego, CA, USA) to yield 10 Gb raw data. Adapter contamination and low-quality reads were filtered, resulting in clean reads ranging from 63M to 73M. Alignment of reads to the human reference genome (hg38) was performed using STAR-2.7.8a.[9] Gene assignments were based on Ensembl 104 build gene models. Counts per million mapped reads (CPM) were generated with Partek Flow software v10.0 (Partek, St. Louis, MO, USA). Gene-specific analysis (GSA) was applied to generate differentially expressed genes (DEGs) using cutoffs of ≥1.5-fold change and FDR<0.05. To curate *NR3C1* isoform expression[10] and hotspot mutations[11] from RNA-seq data, transcript per kilobase million (TPM) normalization and variant calling were respectively performed with Partek Flow.

Quantitative RT-PCR

First-strand cDNA was generated from 500 ng of purified RNA using the High-Capacity cDNA Reverse Transcription Kit (Life Technologies). Quantitative PCRs were set up by mixing 10 ng of cDNA template with TaqMan Gene Expression Master Mix (Life Technologies) and TaqMan assays (Life Technologies). Reactions (50°C, 2 min; 95°C, 10 min; 45 cycles of 95°C, 15 s and 60°C, 1 min) were performed on the QuantStudio 5 Real-Time PCR system (Applied Biosystem). The expression of GC-responsive genes was analyzed by the comparative C_T method and normalized to the expression of *GAPDH*.

Chromatin immunoprecipitation sequencing

Chromatin immunoprecipitation (ChIP) was performed using the SimpleChIP Enzymatic Chromatin IP Kit following the manufacturer's protocols (Cell Signaling Technology). Briefly, Dex-treated BCP-ALL cells were crosslinked with 37% formaldehyde (Sigma-Aldrich) for 10 minutes and quenched with glycine for 5 minutes. Chromatin was isolated from the cell pellets and sonicated to generate 150-900 bp DNA fragments as monitored by agarose gel electrophoresis. Processed chromatin (40 μg) was

immunoprecipitated with control IgG or NR3C1 antibody (clone D8H2, Cell Signaling Technology) at 4°C overnight. DNA was purified from the eluted chromatin, and NGS was performed with the NovoSeq 6000 platform (Illumina) to produce an average of 30 million reads per sample. High quality sequences were mapped to the hg38 reference genome using BWA.[12] Fragment estimation, identification of local noise parameters and peak calling on the aligned reads was performed with MACS3.[13] Peaks indicative of NR3C1 binding were curated and annotated using ChIPseeker.[14,15] Input DNA was used as the background control.

Xenograft experiments

Animal experiments were conducted in accordance with procedures approved by the Institutional Animal Experimentation Ethics Committee. Female NOD.Cg-*Prkdc*^{scid}*Il2rg*^{tm1Wjl}/SzJ (NSG) mice (8-10-week-old; Jackson Laboratory, Bar Harbor, ME, USA) were infused with luciferase-expressing BCP-ALL cells (1×10^6 cells/mouse) *via* tail veins. On day 3 post-infusion, animals were randomized to receive daily administration of vehicle solutions (PBS by intraperitoneal injection and corn oil by oral gavage), Dex (5 mg/kg in PBS by intraperitoneal injection), trametinib (5 mg/kg in corn oil by oral gavage) or their combination.[16] The treatment was performed on a 5 days on and 2 days off schedule for a duration of 2 weeks. When humane endpoints were reached (≥20% weight loss, obvious distress or hindleg paralysis), the systemic leukemic load was evaluated using the IVIS 200 In Vivo Imaging System (Xenogen, Alameda, CA, USA) following the application of D-Luciferin (150 mg/kg; Promega, Madison, WI, USA) and anaesthetization with 2.5% isoflurane (Zowtis, Parippany, NJ, USA). Luminescence signals were captured using the Living Image software (Xenogen). To determine the medullary leukemic burden, single cell suspensions were prepared from the femurs of euthanized animals. After red cell lysis and Fc receptor blocking, leukemic cells were measured by staining with human-specific antibodies against CD19-PE (clone HIB19) and CD45-APC (clone J.33) followed by flow cytometry analyses.

Statistical analyses

The statistical methods applied for individual experiments are indicated in the table footnotes or figure legends. Analyses were performed with GraphPad Prism v8.3.0 (GraphPad) or SPSS v26.0 (IBM Corp, Armonk, NY, USA). *P* values of <0.05 were considered statistically significant.

Supplemental Table 1. Taqman assays

Gene name	Gene symbol	Probe ID
BCL2 like 11	*BCL2L11*	Hs01076940_m1
CD9	*CD9*	Hs00233521_m1
Glyceraldehyde-3-phosphate dehydrogenase	*GAPDH*	Hs99999905_m1
Nuclear receptor subfamily 3 group C member 1	*NR3C1*	Hs00353740_m1
Signal transducer and activator of transcription 5A	*STAT5A*	Hs00559643_m1
TSC22 domain family member 3	*TSC22D3*	Hs00608272_m1
Zinc finger and BTB domain containing 16	*ZBTB16*	Hs00232313_m1

Supplemental Table 2. Characteristics of BCP-ALL samples undergone *ex vivo* drug testing

Sample Code	$CD9^+$ blasts (%)	CD9 group	Gender	Age at diagnosis (years)	Diagnostic WBC ($x10^9$/L)	Response to Pred prephase	Dex IC50 (nM)	Pred IC50 (nM)	Cytogenetics	Gene fusion
Pt_82	0.3	-	M	4.6	5.3	Good	34.1	452	46,XY[24]	*ETV6-RUNX1*
Pt_91	5.2	-	F	2.4	7.0	Poor	>100000	>100000	30,XX,-1,-2,-3,-4,-5,-6,-7,-9,-12,-13,-15,-16,-17,-19,-20,-22[4]/46,XX[20]	NIL
Pt_138	23.9	+	M	11.3	21.3	Good	9.4	172	46,XY,t(12;17)(p13;q21)[9]/47,idem,+del(8)(p21)(4)/47,idem,+1,der(1;15)(q10;q10),+del(8)(p21)[4]/46,XY[6]	NIL
Pt_187	2.2	-	F	9.6	5.4	Good	37.7	326	46,XX[20]	NIL
Pt_238	9.3	-	M	4.1	208.6	Good	5469	15919	46,XY,t(9;22)(q34;q11.20[1]	*BCR-ABL1*
Pt_338	100	+	F	6.3	10.7	N/A	6.8	65.8	46,XX,del(4)(q21q25),del(9)(p22),der(9;12(q10;q10),+mar[17]	NIL
Pt_371	99.9	+	F	3.1	434.6	N/A	30.5	16.6	45,XX,t(9;22)(q34;q11.2),-18[8]/46,XY[2]	*BCR-ABL1*
Pt_372	3.5	-	F	1.2	148.7	N/A	>100000	>100000	46,XX,t(4;11)(q21;q23)[3]/48,idem,+X,+1,-13,i(17)(q10,der(20)t(13;20)(q12;q13.3),+21[5]/46,XX[1]	*KMT2A-AFF1*
Pt_379	100	+	M	12.0	112.0	N/A	59.4	365	47,XY,+X,-6,-9,+mar[17]/46,XY[3]	NIL
Pt_402	88.6	+	M	8.5	12.4	N/A	1119	8445	46,XY,der(1)t(1;1*)(p36.3;q21),t(1;19)(q23;p13.3)[12]/46,XY,t(1;19)(q23;p13.3),-9,+mar[4]/46,XY[4]	*TCF3-PBX1*
Pt_424	97.8	+	M	5.5	72.6	N/A	9.5	90.3	46,XY[20]	NIL
Pt_436	67.7	+	M	6.0	67.0	N/A	104	5874	46,XY,del(4)(q12q12)[5]/46,XY[20]	NIL
Pt_440	38.7	+	M	8.8	3.2	N/A	9.3	83.8	47,XY,del(6)(q21q25),del(11)(q13q23),-12,+16,+mar[8]/47,XY,del(6)(q21q25),add(11)(q23),-12,+16, +mar[6]/46,XY[2]	*ETV6-RUNX1*
Pt_448	99.8	+	M	14.1	87.4	N/A	149	2331	46,XY,del(16)(q12.1)[23]/46,XY[6]	NIL
Pt_453	99.5	+	M	5.8	25.7	N/A	2.4	22.4	46,XY,-18,der(19)t(1;19)(q23;p13.3),+mar[11]/46,idem,add(12)(p11.2)/46,XY[5]	*TCF3-PBX1*
Pt_456	99.5	+	M	5.2	21.1	N/A	3799	17655	53~54,XY,+X[11],+6[11],+10[10],-12[11],+14[11],+14[10],+17[6],+18[10],add(19)(q13.3)[11],+21[11], +21[4],+mar[11][cp11]/46,XY[14]	NIL
Pt_464	98.8	+	F	5.2	3.5	N/A	32.4	518	60<3n>,XX,-X,-1,-2,-4,-9,-11,-12,-13,+14,-15,-16,add(16)(p13.3),-19,-20,+21,+mar[6]/60<3n>,idem, add(11)(q13)[2]/46,XX[9]	NIL
Pt_465	9.4	-	F	8.8	1.2	N/A	53.6	334	46,XX[16]	*ETV6-RUNX1*

Supplemental Table 3. Association of CD9 with clinical characteristics of BCP-ALL patients

Clinical Parameters	All patients (n = 182)		$CD9^+$ patients (n = 146)		$CD9^-$ patients (n = 36)		$CD9^+$ *vs* $CD9^-$
	No.	**%**	**No.**	**%**	**No.**	**%**	***P***
Age, years							
Median (IQR)	4.4 (2.7-7.9)		4.3 (2.6-7.8)		4.8 (2.7-8.0)		0.718
<1	16	8.8	14	9.6	2	5.5	0.742
1 - <10	134	73.6	105	71.9	29	80.6	0.292
≥10	32	17.6	27	18.5	5	13.9	0.516
Sex							
Male	113	62.1	90	61.6	23	63.9	0.804
Female	69	37.9	56	38.4	13	36.1	
WBC, $\times 10^9$/L							
Median (IQR)	13.4 (6.3-54.8)		13.4 (6.3-54.8)		14.2 (6.2-51.3)		0.967
<50	134	73.6	107	73.3	27	75.0	0.835
≥50	48	26.4	39	26.7	9	25.0	
Cytogenetics							
Hyperdiploidy	30	16.5	30	20.5	0	0	***<0.001***
BCR-ABL1	11	6.0	8	5.5	3	8.3	0.457
ETV6-RUNX1	35	19.2	18	12.3	17	47.3	***<0.001***
KMT2A-rearranged	14	7.7	11	7.5	3	8.3	1.000
TCF3-PBX1	10	5.5	10	6.9	0	0	0.215
Others	82	45.1	69	47.3	13	36.1	0.229

Abbreviations: IQR, interquartile range; WBC, white blood cells.
Statistics: continuous variables, Mann-Whitney U test; categorical data, Pearson's Chi-square test or Fisher's exact test.

Supplemental Table 4. Univariate and multivariate analyses of prednisone response

	Univariate			Multivariate		
Variables	**OR**	**95% CI**	***P***	**OR**	**95% CI**	***P***
CD9*						
Positive	1					
Negative	3.7	1.3-10.7	***0.017***	5.1	1.5-17.3	***0.009***
WBC* (× 10^9/L)						
<50	1					
≥50	10.8	3.3-35.6	***<0.001***	13.1	3.7-46.0	***<0.001***
Age (years)						
1-9.9	1					
<1	3.2	0.8-13.3	0.109			
≥10	2.0	0.6-6.9	0.282			
Sex						
Female	1					
Male	1.4	0.5-4.2	0.567			
Hyperdiploidy						
Present	1					
Absent	0.3	0.1-2.5	0.272			
BCR-ABL1*						
Absent	1					
Present	7.6	1.9-29.5	***0.004***	3.4	0.7-17.7	0.145
***KMT2A*-rearrangement**						
Absent	1					
Present	1.8	0.4-9.0	0.456			
TCF3-PBX1						
Absent	1					
Present	1.2	0.1-9.8	0.890			
B-others						
Absent	1					
Present	1.2	0.4-3.5	0.678			

Abbreviations: OR, odds ratio; CI, confidence interval.
Statistics: Multivariate analysis: binary logistic regression model with backward likelihood method.
*Variables included in multivariate analysis.
ETV6-RUNX1 is not included in the analyses because none of the patients were poor prednisone responders.

Supplemental Table 5. Isoform expression and mutational status of *NR3C1* in BCP-ALL cells

Cell type	CD9 group	Dex IC50 (nM)	Pred IC50 (nM)	*NR3C1* Isoform (TPM)			*NR3C1* mutation	
				GRα	GRβ	GRγ	p. Y478C	p. R477H
BCP-ALL cell line								
SEM	low	530	27009	18.7	0	2.3	WT	WT
KOPN-8	low	855	11705	17.2	0	0.8	WT	WT
RS4;11	high	1.1	15.5	73.8	0	5.8	WT	WT
697	high	25.9	421	7.7	0	0.6	WT	WT
SUP-B15	high	3.6	46.7	24.7	0.3	2.4	WT	WT
BV-173	high	5.5	77.6	111	12.3	20.6	WT	WT
Patient sample*								
Pt_82	-	34.1	452	6.1	0	1.8	WT	WT
Pt_91	-	>100000	>100000	9.5	0	2.0	WT	WT
Pt_138	+	9.4	172	18.3	0	4.0	WT	WT
Pt_187	-	37.7	326	12.5	0	1.9	WT	WT
Pt_238	-	5469	15919	15.1	1.3	0.7	WT	WT
Pt_338	+	6.8	65.8	11.9	0	0.9	WT	WT
Pt_371	+	30.5	16.6	17.2	0	2.4	WT	WT
Pt_372	-	>100000	>100000	8.6	0	2.7	WT	WT
Pt_379	+	59.4	365	10.9	3.4	1.3	WT	WT
Pt_402	+	1119	8445	9.7	0	2.4	WT	WT
Pt_424	+	9.5	90.3	9.7	0	2.4	WT	WT
Pt_436	+	104	5874	12.1	0.3	2.4	WT	WT
Pt_440	+	9.3	83.8	40.6	0	7.9	WT	WT
Pt_448	+	149	2331	19.3	0	3.7	WT	WT
Pt_453	+	2.4	22.4	12	0	1.0	WT	WT
Pt_456	+	3799	17655	22.2	0	3.5	WT	WT
Pt_464	+	32.4	518	18.6	0	3.5	WT	WT
Pt_465	-	53.6	334	12.1	0.1	4.2	WT	WT

Abbreviations: TPM, transcripts per kilobase million; WT, wild type.
*****$NR3C1$ isoform expression ($CD9^+$ *vs.* $CD9^-$): GRα, P=0.109; GRβ, P=*0.868*; GRγ, P=0.406.
Statistics: two-tailed, unpaired Student's *t*-test.

Supplemental Table 6. List of differential expressed genes in Dex-treated SEM cells

Gene symbol	FDR step up (CD9-Dexa vs. CD9-DMSO)	Fold change (CD9-Dexa vs. CD9-DMSO)	FDR step up (GFP-Dexa vs. GFP-DMSO)	Fold change (GFP-Dexa vs. GFP-DMSO)	Gene list	Selected gene ontology*	Reported GC responsive genes
SMIM3	3.75E-06	18.518	1.09E-05	16.575	CD9 & GFP		
NDRG2	1.52E-04	10.111	5.81E-03	8.170	CD9 & GFP		Mir *et al*, 2019[17]
ISG20	1.23E-09	7.954	4.84E-09	7.832	CD9 & GFP		Tissing *et al*, 2007[18]
GSDME	7.30E-04	7.558	3.74E-03	6.143	CD9 & GFP		Webb *et al*, 2007[19]
LCN10	6.28E-03	7.532	5.16E-02	6.723	CD9		
EPS8	4.11E-11	6.714	8.65E-10	6.209	CD9 & GFP		
MYRIP	2.62E-11	6.659	2.75E-10	6.147	CD9 & GFP		
FKBP5	1.68E-140	6.035	5.18E-126	5.699	CD9 & GFP		Nold *et al*, 2021[20]
TSC22D3	9.16E-31	5.909	1.40E-24	5.437	CD9 & GFP		Tissing *et al*, 2007[18]
GSN	2.81E-11	5.732	3.21E-11	5.423	CD9 & GFP	Programmed cell death	
SCML4	1.11E-04	5.514	2.36E-04	5.810	CD9 & GFP		
DDIT4	2.04E-43	5.492	1.15E-39	5.317	CD9 & GFP		Wolff *et al*, 2014[21]
LDLRAD4	7.46E-08	5.383	1.18E-06	4.431	CD9 & GFP		
MTUS1	3.42E-07	5.217	5.67E-05	4.121	CD9 & GFP		
XACT	2.11E-04	4.569	1.08E-02	3.172	CD9 & GFP		
GUCY1A2	7.30E-04	4.459	1.21E-01	2.722	CD9		
ADPRHL1	7.60E-03	4.206	1.98E-02	3.716	CD9 & GFP		
FZD4	6.17E-03	3.533	1.16E-01	2.896	CD9		Shi *et al*, 2015[22]
AMOT	2.51E-13	3.411	5.37E-12	3.203	CD9 & GFP		
LONRF1	3.96E-18	3.396	4.33E-12	2.844	CD9 & GFP		
NT5DC2	2.68E-16	3.353	1.43E-11	2.813	CD9 & GFP		
SLC44A1	1.12E-45	3.353	1.23E-39	3.329	CD9 & GFP		
MYO10	8.56E-09	3.228	1.47E-08	3.046	CD9 & GFP		
ZHX3	1.80E-06	3.148	1.69E-06	3.168	CD9 & GFP		
KLF9	3.79E-06	3.037	1.11E-04	2.831	CD9 & GFP		Tissing *et al*, 2007[18]
CRMP1	5.22E-03	2.939	5.60E-03	2.537	CD9 & GFP		
BTNL9	8.52E-03	2.924	1.08E-02	2.933	CD9 & GFP		
RECK	2.19E-03	2.863	1.08E-02	2.713	CD9 & GFP		
ZBTB16	4.85E-02	2.856	3.97E-02	1.980	CD9 & GFP		Tissing *et al*, 2007[18]
AC104530.1	2.77E-04	2.808	1.49E-01	1.962	CD9		
PAG1	1.57E-02	2.775	5.66E-01	1.941	CD9		
CXCR4	4.18E-11	2.745	3.04E-11	2.816	CD9 & GFP		Hong *et al*, 2020[23]
SMAP2	6.85E-08	2.740	2.60E-08	2.938	CD9 & GFP		
IL6ST	5.18E-07	2.708	2.70E-07	2.683	CD9 & GFP		
FGFR1	1.97E-06	2.705	1.18E-06	2.716	CD9 & GFP		Choi *et al*, 2022[24]
DAAM1	2.86E-04	2.700	5.75E-03	2.137	CD9 & GFP		

CLN8	1.52E-04	2.602	4.56E-04	2.866	CD9 & GFP		
HUNK	5.96E-03	2.600	2.74E-03	2.868	CD9 & GFP		
FZD8	8.90E-04	2.569	1.13E-02	2.256	CD9 & GFP		
NFIL3	2.97E-02	2.558	1.55E-01	2.438	CD9		Tissing *et al*, 2007[18]
ANKRD33B	6.17E-09	2.506	9.39E-09	2.526	CD9 & GFP		
MAP3K5	2.47E-06	2.403	3.74E-04	2.092	CD9 & GFP	Programmed cell death	Chen *et al*, 2023[25]
SLC27A3	2.15E-02	2.396	9.83E-02	2.180	CD9		
RASA2	4.48E-03	2.352	5.14E-03	2.382	CD9 & GFP		
NFKBIA	4.79E-03	2.322	3.93E-03	2.321	CD9 & GFP		Zhang *et al*, 2023[26]
CRISPLD1	9.04E-03	2.319	1.37E-02	2.483	CD9 & GFP		
SPRY4	4.96E-02	2.302	3.67E-01	1.847	CD9		
GAB1	8.40E-12	2.297	3.69E-09	2.153	CD9 & GFP		Sharma *et al*, 2015[27]
PER1	6.64E-03	2.258	2.44E-03	2.327	CD9 & GFP	Regulation of glucocorticoid receptor signaling pathway	Yurtsever *et al*, 2019[28]
MGAT4A	5.70E-04	2.240	1.07E-02	1.929	CD9 & GFP		
ZFP36L2	3.78E-12	2.229	9.37E-14	2.429	CD9 & GFP		Tissing *et al*, 2007[18]
CD109	3.96E-17	2.220	3.95E-12	1.962	CD9 & GFP		
USP12	3.78E-09	2.172	5.25E-04	1.702	CD9 & GFP		
IRAK3	1.12E-13	2.152	3.39E-08	1.881	CD9 & GFP		
TMEM65	3.61E-10	2.146	2.95E-07	1.961	CD9 & GFP		
SYNE3	5.45E-10	2.080	2.75E-10	2.136	CD9 & GFP		
INSR	6.62E-20	2.063	4.35E-15	1.905	CD9 & GFP		Tissing *et al*, 2007[18]
KLF7	7.30E-04	2.035	1.90E-03	2.026	CD9 & GFP		
CLNS1A	7.30E-04	1.976	8.39E-02	1.612	CD9		
TGFBR2	3.79E-06	1.928	3.74E-03	1.627	CD9 & GFP		Wang *et al*, 2022[29]
SMARCA2	1.58E-15	1.890	9.78E-12	1.794	CD9 & GFP		
CLMN	7.60E-03	1.881	4.27E-02	1.717	CD9 & GFP		
SYNJ2	1.30E-03	1.877	1.05E-02	1.713	CD9 & GFP		
TACC1	1.17E-06	1.861	2.38E-04	1.661	CD9 & GFP		
SLC44A2	2.39E-06	1.842	1.83E-06	1.827	CD9 & GFP		
BTG1	7.95E-05	1.841	8.47E-03	1.628	CD9 & GFP		Scheijen *et al*, 2017[30]
YBX3	2.84E-06	1.839	2.26E-05	1.791	CD9 & GFP		
BCL2L11	3.79E-06	1.839	4.61E-03	1.584	CD9 & GFP	Programmed cell death	Saenz *et al*, 2015[31]
CTSB	7.30E-04	1.833	5.17E-02	1.624	CD9		
SORT1	7.95E-05	1.829	3.06E-03	1.689	CD9 & GFP		
RASAL2	1.93E-02	1.815	1.29E-01	1.719	CD9		
CD53	1.98E-03	1.808	3.84E-02	1.617	CD9 & GFP		
FOSL2	5.05E-06	1.800	2.57E-06	1.819	CD9 & GFP	Programmed	

						cell death	
REEP3	4.89E-09	1.797	1.42E-04	1.574	CD9 & GFP		
GLUL	7.47E-17	1.788	4.38E-15	1.748	CD9 & GFP		
MAP2K1	3.12E-02	1.781	7.98E-02	1.704	CD9	Response to glucocorticoid	Tissing *et al*, 2007[18]
NISCH	1.02E-04	1.781	2.16E-04	1.802	CD9 & GFP		
WWC3	1.62E-02	1.759	9.58E-02	1.646	CD9		
SNX30	8.40E-12	1.754	3.10E-08	1.618	CD9 & GFP		
MAP3K1	1.41E-06	1.751	2.60E-08	1.903	CD9 & GFP		
KLF13	1.74E-08	1.726	7.08E-06	1.593	CD9 & GFP		Cruz-Topete *et al*, 2016[32]
CD96	7.30E-04	1.714	5.17E-02	1.508	CD9		
NUDT4	1.31E-05	1.701	1.10E-05	1.741	CD9 & GFP		
DOCK7	2.26E-02	1.701	3.00E-01	1.557	CD9		
CSPG4	2.48E-02	1.679	1.90E-03	1.865	CD9 & GFP		
MEF2A	4.30E-06	1.646	1.11E-04	1.572	CD9 & GFP		
OGFRL1	5.54E-03	1.622	2.48E-01	1.427	CD9		Jiang *et al*, 2020[33]
TRAK2	3.98E-02	1.618	1.16E-01	1.574	CD9		
AGO4	2.22E-03	1.603	3.07E-01	1.387	CD9		
LRRFIP1	1.80E-05	1.583	9.19E-05	1.540	CD9 & GFP		
ANAPC16	4.71E-02	1.570	1.34E-01	1.541	CD9		
EZR	1.53E-05	1.537	1.04E-04	1.471	CD9		Tissing *et al*, 2007[18]
TPD52	2.59E-03	1.530	8.91E-03	1.505	CD9 & GFP		
AKAP13	3.48E-03	1.506	6.20E-02	1.406	CD9	Regulation of glucocorticoid receptor signaling pathway	Koide *et al*, 2015[34]
CORO1C	9.15E-03	1.504	4.40E-02	1.431	CD9		
PTK2B	4.43E-05	1.504	4.97E-03	1.400	CD9		
PDE7A	2.69E-02	1.503	3.06E-01	1.422	CD9		Dong *et al*, 2010[35]
RPL41	1.05E-02	-1.501	1.00E+00	-1.005	CD9		
MYO18A	9.86E-03	-1.512	1.13E-02	-1.497	CD9		
H2BC18	5.55E-04	-1.584	1.00E+00	-1.213	CD9		
H4C12	3.98E-02	-1.603	1.00E+00	-1.174	CD9		
FTL	3.40E-03	-1.642	4.68E-01	-1.318	CD9		
CLEC11A	2.05E-03	-1.693	1.24E-01	-1.463	CD9		
RPS11	2.02E-04	-1.708	1.00E+00	-1.095	CD9		
BMF	1.73E-02	-1.766	8.31E-02	-1.667	CD9	Programmed cell death	Chen *et al*, 2010[36]
SASH3	1.90E-02	-1.843	1.39E-01	-1.636	CD9		
TMSB10	2.05E-03	-1.880	9.58E-01	-1.336	CD9		
H2AC7	4.19E-03	-2.830	1.00E+00	-1.114	CD9		

NRP1	1.38E-01	5.834	7.94E-03	6.409	GFP
SPRY1	5.97E-02	4.404	3.84E-02	4.989	GFP
SNX9	5.74E-02	4.808	2.96E-02	4.547	GFP
PLCG1	5.18E-02	2.728	4.77E-03	3.701	GFP
ITGA9	1.28E-01	2.724	2.27E-02	3.442	GFP
LAPTM5	1.83E-06	1.485	1.42E-10	1.602	GFP
SCD	1.30E-02	-1.492	1.54E-02	-1.520	GFP

*****GO annotations[37,38].

Supplemental Figure 1

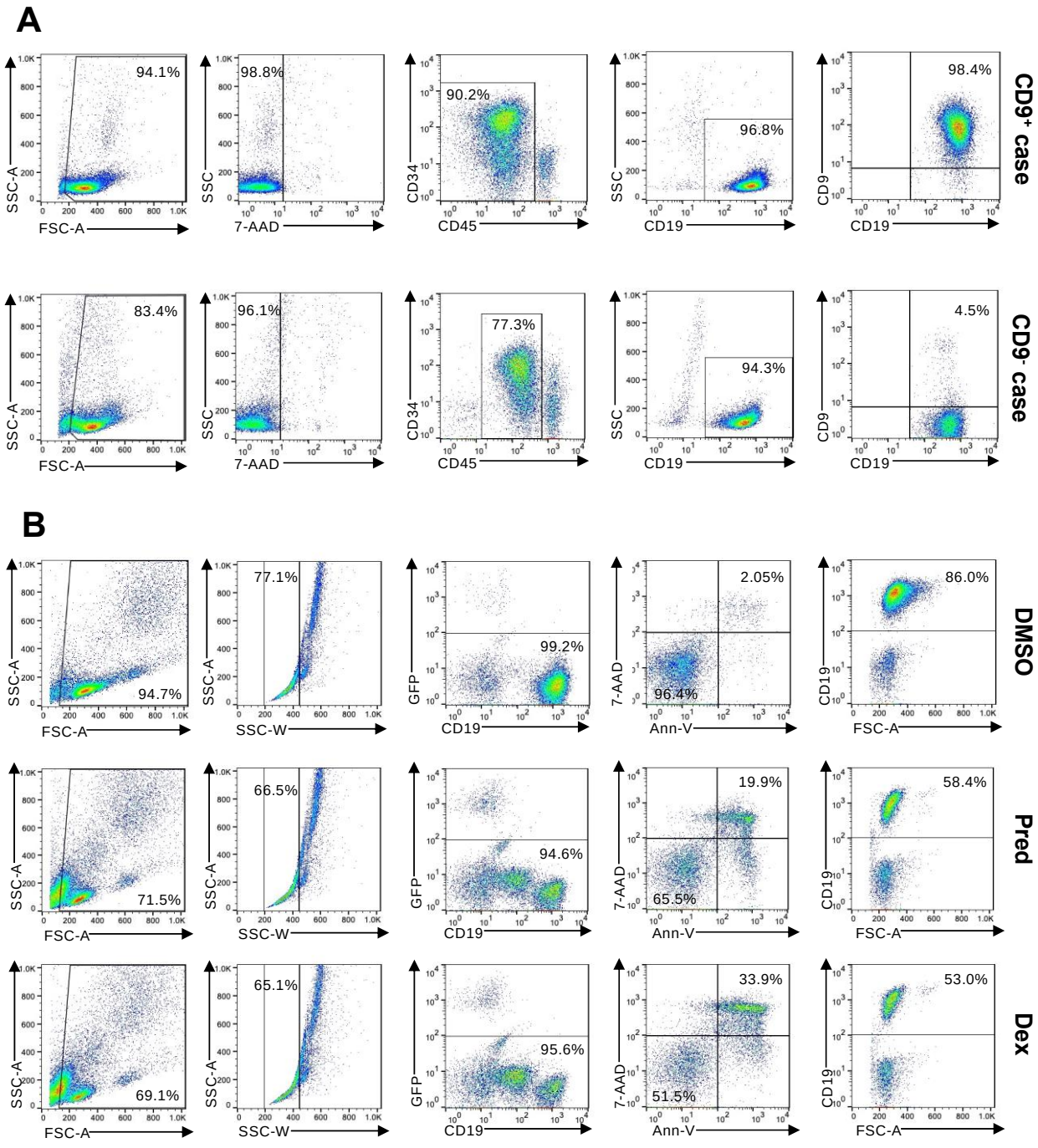

Supplemental Figure 1. Gating strategy for determination of CD9 expression and apoptosis in pediatric BCP-ALL samples. (A) Lymphoblasts were identified by light scattering properties with 7-AAD$^+$ cells excluded for analyses. CD45$^{dim/-}$CD34$^{+/-}$CD19$^+$ leukemic blasts were analyzed for CD9 expression with reference to the isotype controls. The sequential gating strategies of a CD9$^+$ (upper) and a CD9$^-$ (lower) case are shown. Positivity was defined by the presence of ≥20% CD9$^+$ blasts. (B)

Leukemic blasts in hTERT-MSC cocultures were identified by light scattering properties, followed by singlet selection by SSC parameters. GFP^- lymphoblasts were distinguished from GFP^+ MSCs and quantified for viable cells with Annexin $V^-/7\text{-}AAD^-$ phenotype. Viable lymphoblasts were further validated for CD19 expression. Shown are representative flow cytometry plots of a BCP-ALL sample treated with DMSO control, Dex (0.1 μM) or Pred (10 μM). Abbreviations: 7-AAD, 7-actino-aminomycin D; FSC, forward scatter; SSC, side scatter.

Supplemental Figure 2

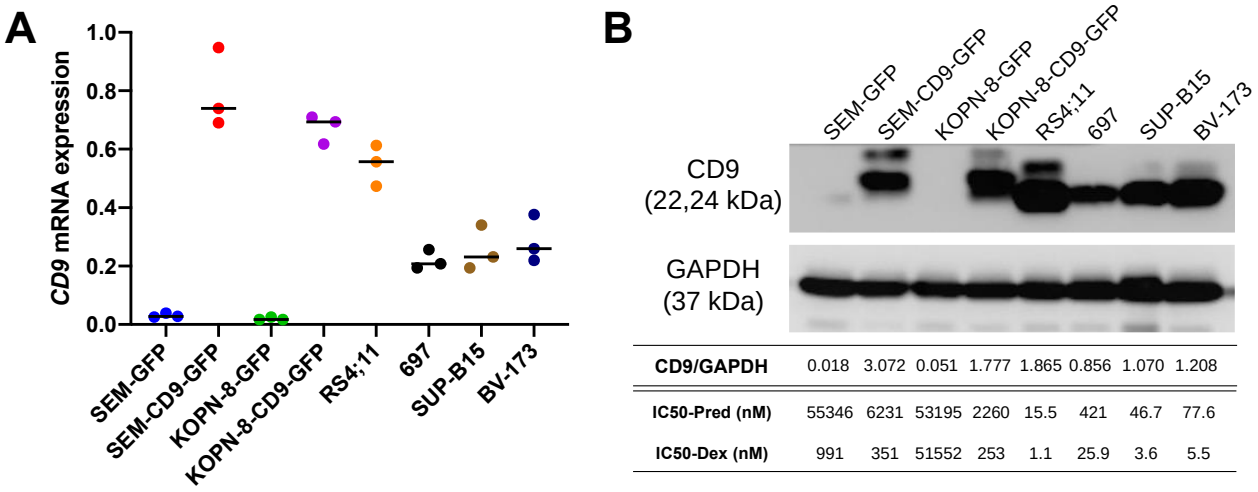

CD9/GAPDH	0.018	3.072	0.051	1.777	1.865	0.856	1.070	1.208
IC50-Pred (nM)	55346	6231	53195	2260	15.5	421	46.7	77.6
IC50-Dex (nM)	991	351	51552	253	1.1	25.9	3.6	5.5

Supplemental Figure 2. Comparison of CD9 expression and GC sensitivity among CD9-overexpressing and inherently CD9^{high} BCP-ALL cells. (A) *CD9* mRNA levels in CD9-transduced versus CD9^{high} BCP-ALL cells as determined by qRT-PCR (n=3). Expression was normalized to *GAPDH*. (B) CD9 protein levels in CD9-transduced versus CD9^{high} BCP-ALL cells as determined by Western blotting. Shown are representative images of 2 independent measurements. CD9/GAPDH ratio and Pred/Dex IC50s are indicated.

Supplemental Figure 3

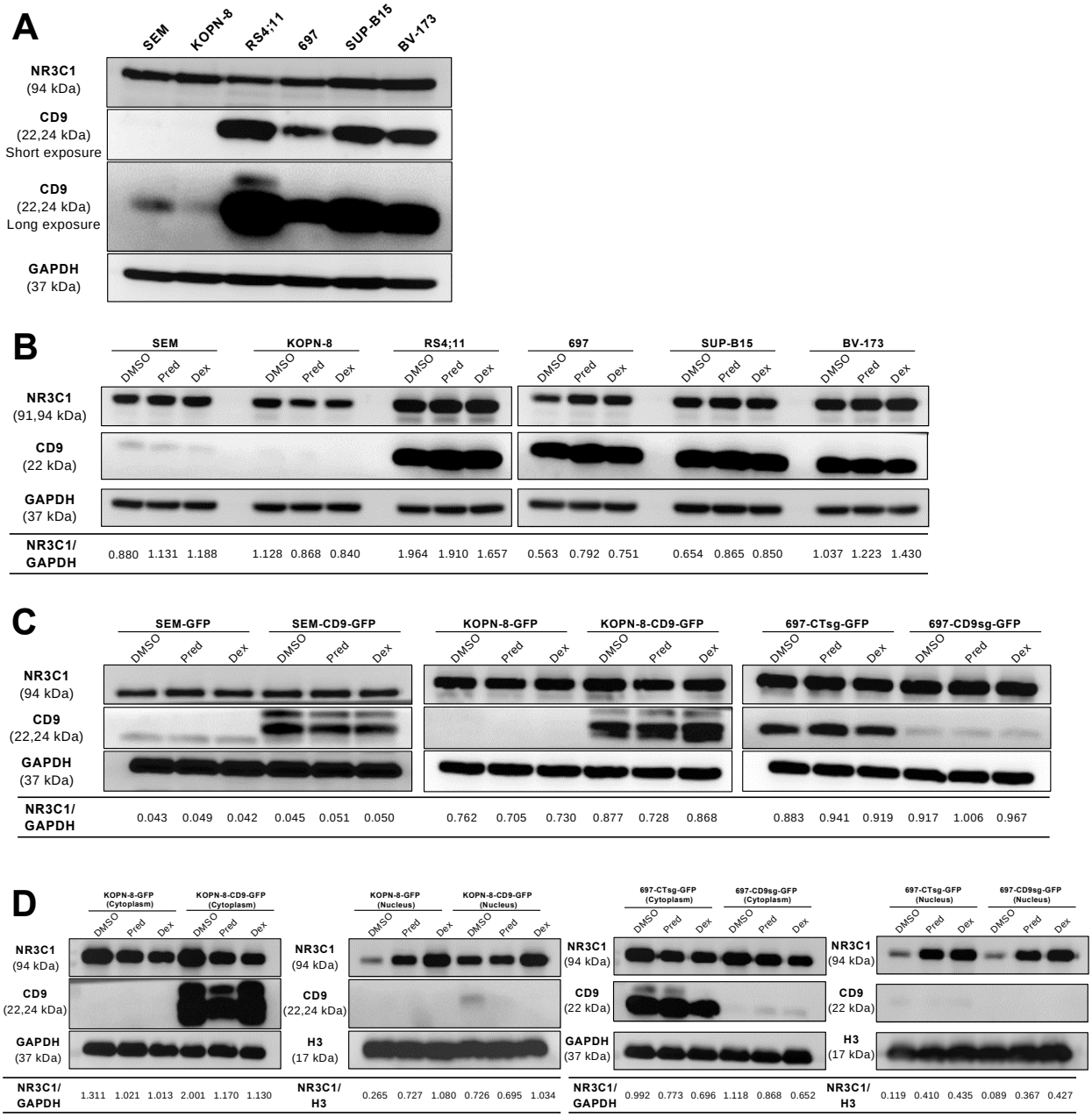

Supplemental Figure 3. CD9 does not affect the expression or nuclear translocation of NR3C1. (A) Expression of total NR3C1 in (A) $CD9^{high}$ (n=4) or $CD9^{low}$ (n=2) BCP-ALL cell lines as revealed by Western blotting, with GAPDH as the internal control. (B) Parental BCP-ALL cell lines were treated with respective IC50 concentrations of Pred (SEM, 30 μM; KOPN-8, 15 μM; RS4;11, 0.02 μM; 697, 0.5 μM; SUP-B15, 0.05 μM; BV-173, 0.1 μM) or Dex (SEM, 0.5 μM; KOPN-8, 1 μM; RS4;11, 0.001 μM; 697, 0.03 μM; SUP-B15, 0.005 μM; BV-173, 0.005 μM) for 8 hours. (C,D) Transduced BCP-ALL cell lines were treated with respective IC50 concentrations of Pred (SEM, 50 μM; KOPN-8, 50

μM; 697; 0.3 μM) or Dex (SEM, 1 μM; KOPN-8, 50 μM; 697, 0.02 μM) for 8 hours. The expression level of NR3C1 in (B,C) whole cell lysates or (D) fractionated cell lysates was measured by Western blotting. NR3C1/GAPDH or NR3C1/H3 intensity ratios are indicated.

Supplemental Figure 4

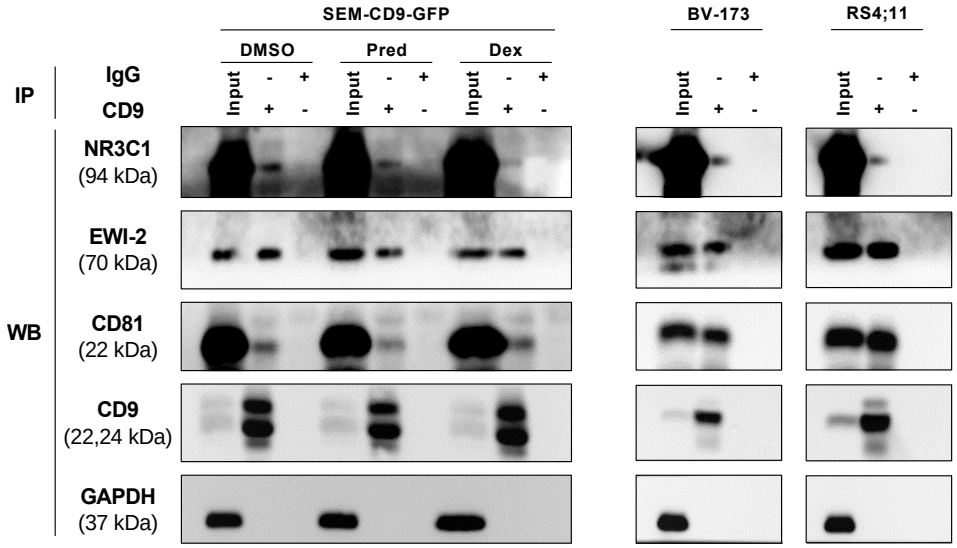

Supplemental Figure 4. NR3C1 physically interacts with CD9 in the tetraspanin-enriched microdomain. Transduced SEM-CD9-GFP as well as inherently $CD9^{high}$ BV-173 and RS4;11 BCP-ALL cells were treated with DMSO, Pred (50μM) or Dex (1μM) for 8 hours. Lysates were immunoprecipitated with IgG_{2b} or anti-CD9, and probed with antibodies against NR3C1 and the well-known TEM components EWI-2 and CD81. The presented images are representative of 3 independent experiments.

Supplemental Figure 5

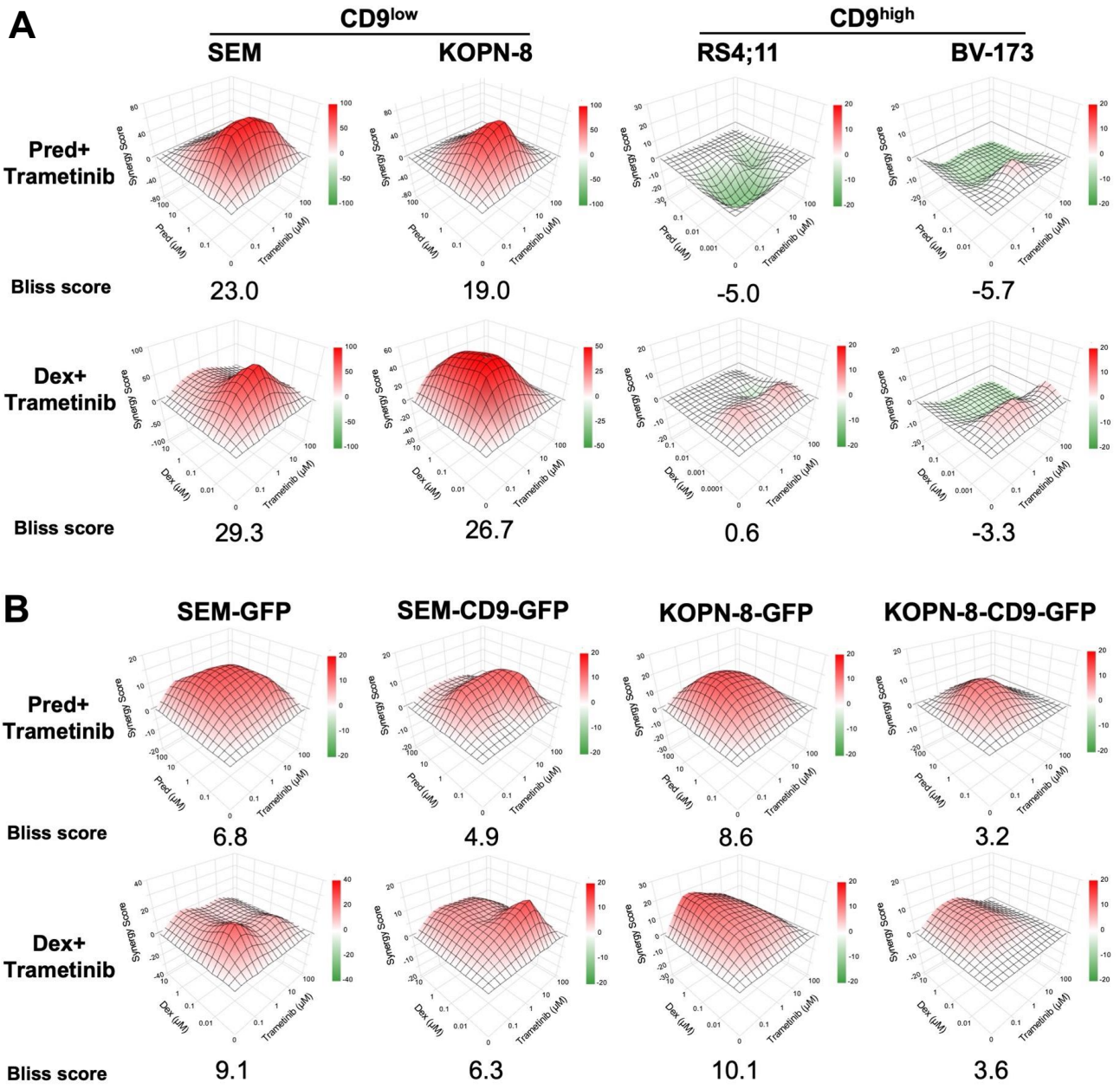

Supplemental Figure 5. MEK inhibitor synergistically increases the vulnerability of CD9^{low} BCP-ALL cells to GCs. (A) CD9^{low} (SEM, KOPN-8) and CD9^{high} (RS4;11, BV-173) BCP-ALL cells as well as (B) CD9-transduced cells were treated with combinations of trametinib (0.1 μM-100 μM) and Pred (1 nM-100 μM) or Dex (0.1 nM-10 μM) for 72 hours. For parental cells, the dose ranges of GCs were determined by their respective IC50s to ensure optimal model fitting. Drug interactions were calculated by the Bliss independence model, with relative cell viability normalized to DMSO controls as the experimental variable. The synergy map simulates the mode of drug interaction, with the color

bar indicating the excess over Bliss score at individual combinations. The overall mean Bliss scores of the combinations are indicated at the bottom: >0, overall synergy; =0, independence; <0, overall antagonism.

Supplemental Figure 6

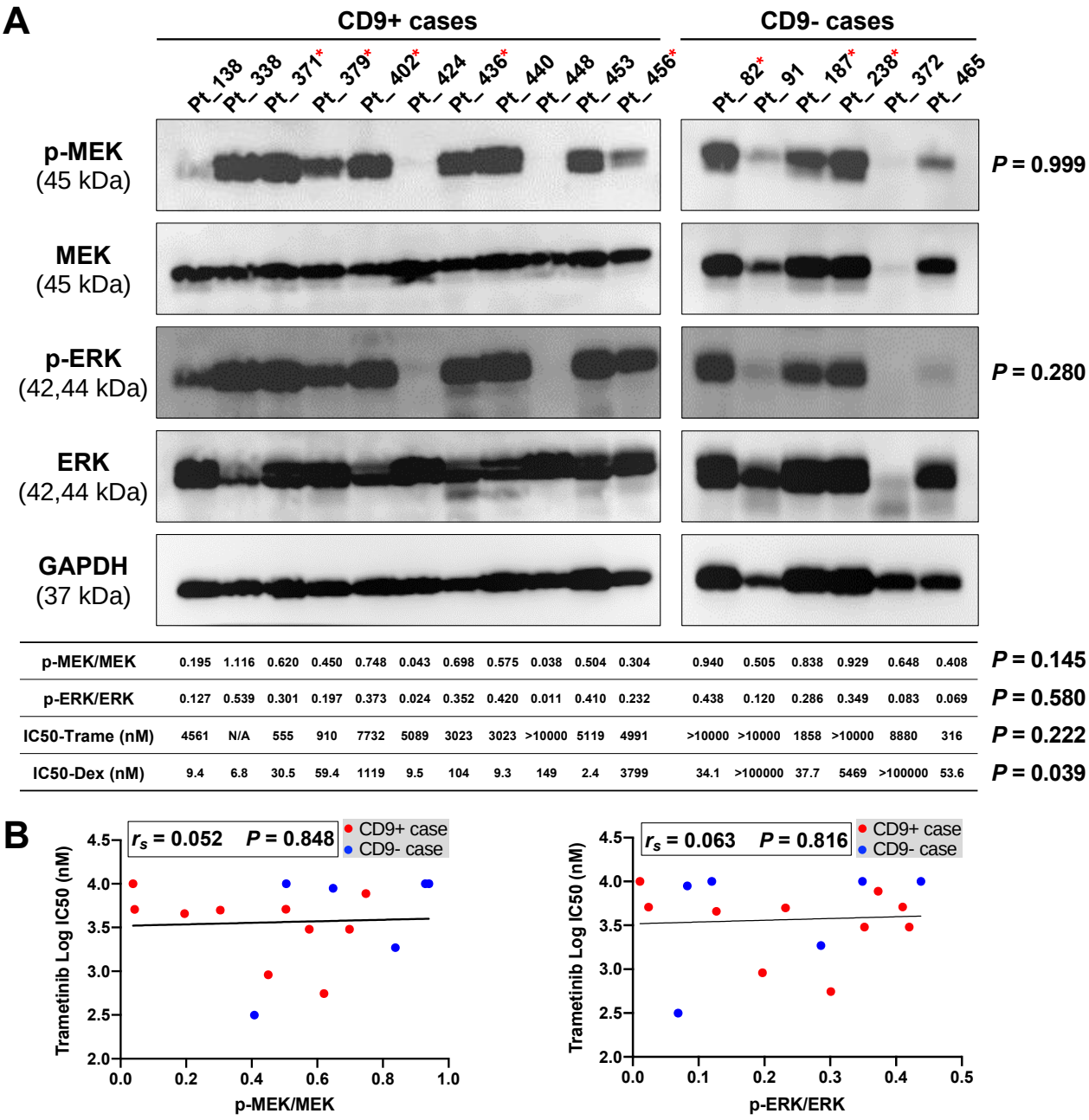

Supplemental Figure 6. Sensitivity of BCP-ALL cells to trametinib could not be predicted by activation status of MEK or ERK. (A) Basal expression level of key MAPK pathway components in BCP-ALL samples ($CD9^+$, n=11; $CD9^-$, n=6) as measured by Western blotting. Annotated are the normalized levels of p-MEK and p-ERK as well as the IC50s of trametinib and Dex of each sample. Asterisks denote samples chosen for drug combination experiments. (B) Correlation of MEK/ERK activation status with trametinib sensitivity. Statistics: (A) Fisher's exact test for comparing the p-MEK and p-ERK status between $CD9^+$ and $CD9^-$ cases; two-tailed, unpaired Student's *t*-test for

comparing the p-MEK/MEK and p-ERK/ERK ratio as well as trametinib and Dex sensitivity between $CD9^+$ and $CD9^-$ cases; (B) Spearman's correlation for determining the association of MEK and ERK activation with trametinib sensitivity.

Supplemental References

1. Lee SHR, Yang W, Gocho Y, et al. Pharmacotypes across the genomic landscape of pediatric acute lymphoblastic leukemia and impact on treatment response. Nat Med. 2023;29(1):170–179.
2. Wang H, Chan KYY, Cheng CK, et al. Pharmacogenomic profiling of pediatric acute myeloid leukemia to identify therapeutic vulnerabilities and inform functional precision medicine. Blood Cancer Discov. 2022;3(6):516–535.
3. Zhou Q, Yang J-J, Chen Z-H, et al. Serial cfDNA assessment of response and resistance to EGFR-TKI for patients with EGFR-L858R mutant lung cancer from a prospective clinical trial. J Hematol Oncol. 2016;9(1):86.
4. Ianevski A, Giri AK, Aittokallio T. SynergyFinder 2.0: visual analytics of multi-drug combination synergies. Nucleic Acids Res. 2020;48(W1):W488–W493.
5. Li CK, Chik KW, Ha SY, et al. Improved outcome of acute lymphoblastic leukaemia treated by delayed intensification in Hong Kong children: HKALL97 study. Hong Kong Med J. 2006;12(1):33–39.
6. Stary J, Zimmermann M, Campbell M, et al. Intensive chemotherapy for childhood acute lymphoblastic leukemia: Results of the randomized intercontinental trial ALL IC-BFM 2002. J Clin Oncol. 2014;32(3):174–184.
7. Cui L, Li ZG, Chai YH, et al. Outcome of children with newly diagnosed acute lymphoblastic leukemia treated with CCLG-ALL 2008: The first nation-wide prospective multicenter study in China. Am J Hematol. 2018;93(7):913–920.
8. Chan KYY, Zhang C, Wong YTS, et al. R4 RGS proteins suppress engraftment of human hematopoietic stem/progenitor cells by modulating SDF-1/CXCR4 signaling. Blood Adv. 2021;5(21):4380–4392.
9. Dobin A, Davis CA, Schlesinger F, et al. STAR: ultrafast universal RNA-seq aligner. Bioinformatics. 2013;29(1):15–21.
10. Zhang C, Zhang B, Lin L-L, Zhao S. Evaluation and comparison of computational tools for RNA-seq isoform quantification. BMC Genomics. 2017;18(1):583.
11. Liu T, Rao J, Hu W, et al. Distinct genomic landscape of Chinese pediatric acute myeloid leukemia impacts clinical risk classification. Nat Commun. 2022;13(1):1640.
12. Li H, Durbin R. Fast and accurate short read alignment with Burrows-Wheeler transform. Bioinformatics. 2009;25(14):1754–1760.
13. Zhang Y, Liu T, Meyer CA, et al. Model-based analysis of ChIP-Seq (MACS). Genome Biol. 2008;9(9):R137.
14. Wang Q, Li M, Wu T, et al. Exploring Epigenomic Datasets by ChIPseeker. Curr Protoc. 2022;2(10):e585.
15. Yu G, Wang L-G, He Q-Y. ChIPseeker: an R/Bioconductor package for ChIP peak annotation, comparison and visualization. Bioinformatics. 2015;31(14):2382–2383.
16. Kerstjens M, Pinhancos SS, Castro PG, et al. Trametinib inhibits RAS-mutant MLL-rearranged acute lymphoblastic leukemia at specific niche sites and reduces ERK phosphorylation in vivo. Haematologica. 2018;103(4):e147–e150.
17. Mir BA, Islam R, Kalanon M, Russell AP, Foletta VC. MicroRNA suppression of stress-responsive NDRG2 during dexamethasone treatment in skeletal muscle cells. BMC Mol Cell Biol. 2019;20(1):12.
18. Tissing WJE, den Boer ML, Meijerink JPP, et al. Genomewide identification of prednisolone-responsive genes in acute lymphoblastic leukemia cells. Blood. 2007;109(9):3929–3935.
19. Webb MS, Miller AL, Thompson EB. In CEM cells the autosomal deafness gene dfna5 is regulated by glucocorticoids and forskolin. J Steroid Biochem Mol Biol. 2007;107(1–2):15–21.
20. Nold V, Richter N, Hengerer B, Kolassa IT, Allers KA. FKBP5 polymorphisms induce differential

glucocorticoid responsiveness in primary CNS cells – First insights from novel humanized mice. Eur J Neurosci. 2021; 53(2):402-415.
21. Wolff NC, McKay RM, Brugarolas J. REDD1/DDIT4-independent mTORC1 inhibition and apoptosis by glucocorticoids in thymocytes. Mol Cancer Res. 2014;12(6):867–877.
22. Shi C, Huang P, Kang H, et al. Glucocorticoid inhibits cell proliferation in differentiating osteoblasts by microRNA-199a targeting of WNT signaling. J Mol Endocrinol. 2015;54(3):325–337.
23. Hong SG, Sato N, Legrand F, et al. Glucocorticoid-induced eosinopenia results from CXCR4-dependent bone marrow migration. Blood. 2020;136(23):2667–2678.
24. Choi GE, Chae CW, Park MR, et al. Prenatal glucocorticoid exposure selectively impairs neuroligin 1-dependent neurogenesis by suppressing astrocytic FGF2-neuronal FGFR1 axis. Cell Mol Life Sci. 2022;79(6):294.
25. Chen N, Meng Y, Zhan H, Li G. Identification and Validation of Potential Ferroptosis-Related Genes in Glucocorticoid-Induced Osteonecrosis of the Femoral Head. Medicina (Kaunas). 2023;59(2):297.
26. Zhang Q, Sun C, Liu X, Zhu C, Ma C, Feng R. Mechanism of immune infiltration in synovial tissue of osteoarthritis: a gene expression-based study. J Orthop Surg. 2023;18(1):58.
27. Sharma A, Menche J, Huang CC, et al. A disease module in the interactome explains disease heterogeneity, drug response and captures novel pathways and genes in asthma. Hum Mol Genet. 2015;24(11):3005–3020.
28. Yurtsever T, Streit F, Foo JC, et al. Temporal dynamics of cortisol-associated changes in mRNA expression of glucocorticoid responsive genes FKBP5, GILZ, SDPR, PER1, PER2 and PER3 in healthy humans. Psychoneuroendocrinology. 2019;10263–10267.
29. Wang X, Li Q, Li W, et al. Dexamethasone attenuated thoracic aortic aneurysm and dissection in vascular smooth muscle cell Tgfbr2-disrupted mice with CCL8 suppression. Exp Physiol. 2022;107(6):631–645.
30. Scheijen B, Boer JM, Marke R, et al. Tumor suppressors BTG1 and IKZF1 cooperate during mouse leukemia development and increase relapse risk in B-cell precursor acute lymphoblastic leukemia patients. Haematologica.2017;102(3):541-551.
31. Saenz GJ, Hovanessian R, Gisis AD, Medh RD. Glucocorticoid-mediated co-regulation of RCAN1-1, E4BP4 and BIM in human leukemia cells susceptible to apoptosis. Biochem Biophys Res Commun. 2015;463(4):1291–1296.
32. Cruz-Topete D, He B, Xu X, Cidlowski JA. Krüppel-like Factor 13 Is a Major Mediator of Glucocorticoid Receptor Signaling in Cardiomyocytes and Protects These Cells from DNA Damage and Death. J Biol Chem. 2016;291(37):19374–19386.
33. Jiang D, Jin H, Zuo J, et al. Potential biomarkers screening to predict side effects of dexamethasone in different cancers. Mol Genet Genomic Med. 2020;8(4):e1160.
34. Koide H, Holmbeck K, Lui JC, et al. Mice Deficient in AKAP13 (BRX) Are Osteoporotic and Have Impaired Osteogenesis. J Bone Miner Res. 2015;30(10):1887–1895.
35. Dong H, Zitt C, Auriga C, Hatzelmann A, Epstein PM. Inhibition of PDE3, PDE4 and PDE7 potentiates glucocorticoid-induced apoptosis and overcomes glucocorticoid resistance in CEM T leukemic cells. Biochem Pharmacol. 2010;79(3):321–329.
36. Chen DW-C, Lynch JT, Demonacos C, Krstic-Demonacos M, Schwartz J-M. Quantitative analysis and modeling of glucocorticoid-controlled gene expression. Pharmacogenomics. 2010;11(11):1545–1560.
37. Ashburner M, Ball CA, Blake JA, et al. Gene Ontology: tool for the unification of biology. Nat Genet. 2000;25(1):25–29.
38. Aleksander SA, Balhoff J, Carbon S, et al. The Gene Ontology knowledge base in 2023. Genetics. 2023;224(1):iyad031.